U.PORTO

MESTRADO

NEUROBIOLOGIA

DISSECTING THE MOLECULAR CAUSES OF *NDE1*-ASSOCIATED MICROCEPHALY

Cármen Leal Vieira

M

2019

U.PORTO

Cármen Leal Vieira. DISSECTING THE MOLECULAR CAUSES OF *NDE1*-ASSOCIATED MICROCEPHALY

DISSECTING THE MOLECULAR CAUSES OF *NDE1*-ASSOCIATED MICROCEPHALY

Cármen Leal Vieira

FACULDADE DE MEDICINA

M.FMUP **2019**

U.PORTO

MESTRADO
NEUROBIOLOGIA

DISSECTING THE MOLECULAR CAUSES OF *NDE1*-ASSOCIATED MICROCEPHALY

Cármen Leal Vieira

M

2019

DISSECTING THE MOLECULAR CAUSES OF *NDE1*-ASSOCIATED MICROCEPHALY

Tese de Candidatura ao grau de Mestre em Neurobiologia submetida à Faculdade de Medicina da Universidade do Porto (FMUP)

Orientador – Doutor Tiago J. Dantas

IBMC – Instituto de Biologia Molecular e Celular,
I3S – Instituto de Investigação e Inovação em Saúde,
Universidade do Porto, Porto, Portugal.

This work was financed by FEDER - Fundo Europeu de Desenvolvimento Regional funds through the COMPETE 2020 - Operacional Programme for Competitiveness and Internationalisation (POCI), Portugal 2020, and by Portuguese funds through FCT - Fundação para a Ciência e a Tecnologia/Ministério da Ciência, Tecnologia e Ensino Superior in the framework of the project POCI-01-0145-FEDER-029471.

ACKNOWLEDGEMENTS

First, I would like to thank my supervisor Dr. Tiago Dantas, for the persistent guidance and help during the past year. I am particularly grateful for all the scientific knowledge and scientific discussions (especially the “things no one tells you”), which allowed me to grow a little more as a research scientist. In addition, doing this thesis with him allowed me to try many different techniques and expand my horizons.

I would like to express my gratitude for all members of Cell Division Mechanisms and Cytoskeletal Dynamics groups, who kindly received me in the GC lab and were always willing to answer any questions. Special thanks to our TD team for all the help. As a first member, I could see the team grow and develop a good work environment, which made me very motivated.

Additionally, I would like to thank the members of FMUP Biomedicine department, especially Dr. Filipe Monteiro, for allowing us to use important equipment and Dr. Carlos Reguenga (MeN headmaster), for all the feedback during this thesis . Also, I want to thank Dr. Neide Veira (ICVS-Braga) and i3S Histology and Electron Microscopy platform, for the experiments performed that were included in this thesis.

To my friends: my fellow MeN master colleagues “Agrobetos” (especially my i3S mates Inês and Lisboeta David), my meme colleagues “Lab Rookies” and my Scouts friends, who had to put up with me during this thesis thank you for the lunches, coffees, messages and laughs.

At last but certainly not least, I want to express gratitude to my parents for their constant support and encouragement. This master would not have been possible without them. Obrigada mãe e pai!

ABSTRACT

Microcephaly is a neurological condition characterized by a marked reduction in the brain neocortex and head size. This can result from problems in the proliferation, migration and neurogenesis of embryonic neural stem cells, known as radial glial progenitors (RGPs). In severe cases of microcephaly, such as those associated with mutations in the *NDE1* gene (encoding a Dynein-1 regulator), RGPs become trapped at multiple stages of the cell cycle, losing their ability to generate new cells. Two of these arrests have been well characterized by others and are linked with defects in Dynein-1-driven nuclear migration and mitotic entry. The third, less understood *NDE1*-associated arrest occurs in G1 and seems to be related with defects in primary cilium resorption/ signaling. This work aims to better understand the mechanisms underlying this arrest using *in utero* electroporation of rat embryos. We expressed NDE1 point mutants specifically incapable of binding Dynein-1 or LIS1 to attempt to separate functions while co-depleting NDE1 and its paralog NDE1-like in neural progenitors.

In order to better dissect the effects of NDE1 loss in cilia function, we used *C. elegans* as a complementary model, where cilia are dispensable for survival but are essential for key functions in sensory neurons. Assembly and functions of all cilia rely on intraflagellar transport (IFT), a specialized movement of cargoes from the base to the tip of the cilium and back. Interestingly retrograde IFT is driven by Dynein-2, a minus ended-directed motor structurally very similar to Dynein-1. Taking this into account, we hypothesized that, in addition to Dynein-1, NDE1 might also regulate Dynein-2 and therefore ciliogenesis or cilium-dependent signaling. Using a knockout strain of the *NDE1* ortholog *nud-2*, we performed live fluorescence microscopy to study the contribution of NUD-2 for cilia formation, Dynein-2-mediated transport and sensory cilia functions.

Our results suggest that LIS1 is required for all NDE1 functions in the RGPs cell cycle, including the cilium-dependent G1-to-S transition. In contrast, it seems that NDE1 works independently of Dynein-1 in the regulation of this particular cell cycle transition. We also found that loss of the NDE1 ortholog in *C. elegans,* NUD-2, does not greatly perturb cilia length, Dynein-2 recruitment or cilia-mediated

processes, but nonetheless alters distribution of cargoes along cilia and affects velocity of IFT transport.

Altogether, our results using two complementary model systems provide important new insights into how NDE1 contributes to the functions of cytoplasmic Dyneins during brain development.

KEYWORDS

NDE1, brain development, cytoplasmic Dynein motor, cilia, neural progenitors

RESUMO

Microcefalia é uma condição neurológica caracterizada por uma redução acentuada no neocórtex cerebral e no tamanho da cabeça. Esta patologia pode resultar de problemas na proliferação, migração e neurogénese das células estaminais neuronais embrionárias, conhecidas como progenitores da glia radial (RGPs). Em casos graves de microcefalia, como aqueles associados a mutações no gene NDE1 (que codifica um regulador da Dineína-1), as RGPs ficam presas em várias fases do ciclo celular, perdendo a capacidade de gerar novas células. Dois destes bloqueios no ciclo celular estão associados a defeitos na função da Dineína-1 na migração nuclear e na entrada em mitose. O terceiro bloqueio que ocorre na fase G1 do ciclo celular está relacionado com defeitos na reabsorção / sinalização mediada pelo cílio primário, embora o mecanismo seja menos compreendido. Este trabalho teve como objetivo o estudo dos mecanismos subjacentes à paragem do ciclo celular em G1, utilizando eletroporação in utero de embriões de rato. Para isso, nós expressamos mutantes de NDE1 especificamente incapazes de se ligar à Dineína-1 ou LIS1, a fim de tentar separar as funções destas proteínas, aquando da perda de NDE1 e NDEL1.

Utilizamos *C. elegans* como modelo complementar para dissecar os efeitos da perda de NDE1 na função dos cílios uma vez que estes são dispensáveis para a sobrevivência, mas essenciais para funções específicas nos neurónios sensoriais. A formação e funcionamento de todos os cílios dependem de um mecanismo designado transporte intraflagelar (IFT), que consiste no movimento de cargas da base à ponta do cílio e vice-versa. Curiosamente, o IFT retrógrado (no sentido da polarização negativa dos microtúbulos) é realizado pela Dineína-2, um motor estruturalmente muito semelhante à Dineína-1. Tendo isto em consideração, nós hipotetizamos que, para além de regular a Dineína-1, a NDE1 também poderá regular a Dineína-2 e, portanto, a ciliogénese ou sinalização dependente dos cílios. Para estudar isto, nós usamos uma estirpe knockout do ortólogo de NDE1 (nud-2), e, por microscopia de fluorescência estudamos a contribuição da NUD-2 na formação de cílios, no transporte mediado por Dineína-2 e nas funções sensoriais dos cílios.

Os nossos resultados sugerem que a LIS1 é necessária para todas as funções da NDE1, no ciclo celular das RGPs, incluindo na transição de G1 para S, que é dependente dos cílios. Por outro lado, parece que a NDE1 funciona independentemente da Dineína-1, na regulação desta transição do ciclo celular. Neste projeto também descobrimos que a perda do ortólogo da NDE1 em *C. elegans*, NUD-2, não altera substancialmente o comprimento dos cílios, o recrutamento de Dineína-2 ou os processos mediados por cílios. No entanto, detetámos que a perda de NUD-2 altera a distribuição de cargas ao longo dos cílios e influencia a velocidade do transporte IFT.

Em suma, os nossos resultados obtidos com dois modelos complementares originaram novas perspetivas sobre a contribuição da NDE1 nas funções de Dineínas citoplasmáticas, durante o desenvolvimento cerebral.

PALAVRAS-CHAVE

NDE1, desenvolvimento cerebral, motor Dineína citoplasmático, cílios, progenitores neuronais

LIST OF ABBREVIATIONS

AAA+	ATPases associated with diverse activities
ATP	Adenosine triphosphate
BicD2	Protein bicaudal D homolog 2
bp	Base-pair
C. elegans	*Caenorhabditis elegans*
CAG	Cytomegalovirus enhancer, actin promoter and Globin splice acceptor site
CNS	Central nervous system
CP	Cortical plate
CR	Polymerase chain reaction
DAPI	4′,6-diamidino-2-phenylindole
DNA	Deoxyribonucleic acid
E. coli	*Escherichia coli*
E19	Embryonic day 19
FW	Forward
G1	Growth 1 / Gap 1 Phase
G2	Growth 2 / Gap 2 Phase
GFP	Green Fluorescent Protein
HC	Heavy chain
IC	Intermediate chain
IFT	Intraflagellar transport
IFT-A	IFT subcomplex A
IFT-B	IFT subcomplex-B
INM	Interkinetic nuclear migration
IRES	Internal ribosome entry site
KD	Knockdown
kDa	kilodalton
KO	Knockout
L1	Larval stage 1

LC	Light chain
LIC	Light intermediate chain
LIS1	Lissencephaly 1 Protein, also known as NudF
M-phase	Mitotic Phase
mRNA	Messenger RNA
MTOC	Microtubule organizing center
MTs	Microtubules
N.A	Numerical aperture
NDE1	Nuclear Distribution Protein NudE Homolog 1
NDEL1	Nuclear Distribution Protein NudE-Like 1
NE	Nuclear envelope
NGM	Nematode growth medium
OE	Overexpression
PBS	Phosphate-Buffered Saline
PFA	Paraformaldehyde
RFP	Red fluorescent protein
RGPs	Radial glial progenitors
RNA	Ribonucleic acid
RT	Room temperature
RV	Reverse
shRNA	Short hairpin RNA
S-phase	Synthesis Phase
SVZ	Subventricular zone
TAE	Tris-Acetate-EDTA
TEM	Transmission electron microscopy
VS	Ventricular surface
VZ	Ventricular zone
WT	Wild type

LIST OF FIGURES

LIST OF TABLES

TABLE OF CONTENTS

INTRODUCTION

1. BRAIN AND NERVOUS SYSTEM DEVELOPMENT

All animals begin life as a single cell that undergoes countless divisions and differentiation processes to ultimately form a system, in which interacting parts form a unified whole.

The nervous system begins to develop at a later stage of embryogenesis and it is only completed after birth. This spawns the most complex organ within the human embryo – the brain [1, 2].

The first steps in brain and nervous system development start with emergence of neural stem cells (or neural progenitors) in the ectoderm, the outermost layer of the three-layered gastrula. As development progresses, neural progenitor cells will accumulate in the neural plate, that will fold and invaginate to eventually establish a neural tube, the first well defined neural structure **(Fig. 1A)** [2].

As the pseudostratified epithelium of the neural tube becomes larger and more complex, more neural progenitors elongate their processes: cells elongate an apical process to the ventricular surface and a basal process that reaches the pial surface of the brain **(Fig. 1A and 1B)**, at which stage they are referred to as radial glial progenitors (RGPs). [1].

RGPs give rise to nearly all cortical neurons and glial cells and serve as scaffolds for neuronal migration **(Fig. 1C)** [3]. Symmetric division of RGPs leads to formation of two additional progenitor cells and, therefore, an increase in their pool, whereas asymmetric division can yield a neuron, an intermediate progenitor or a short neural precursor [3, 4].

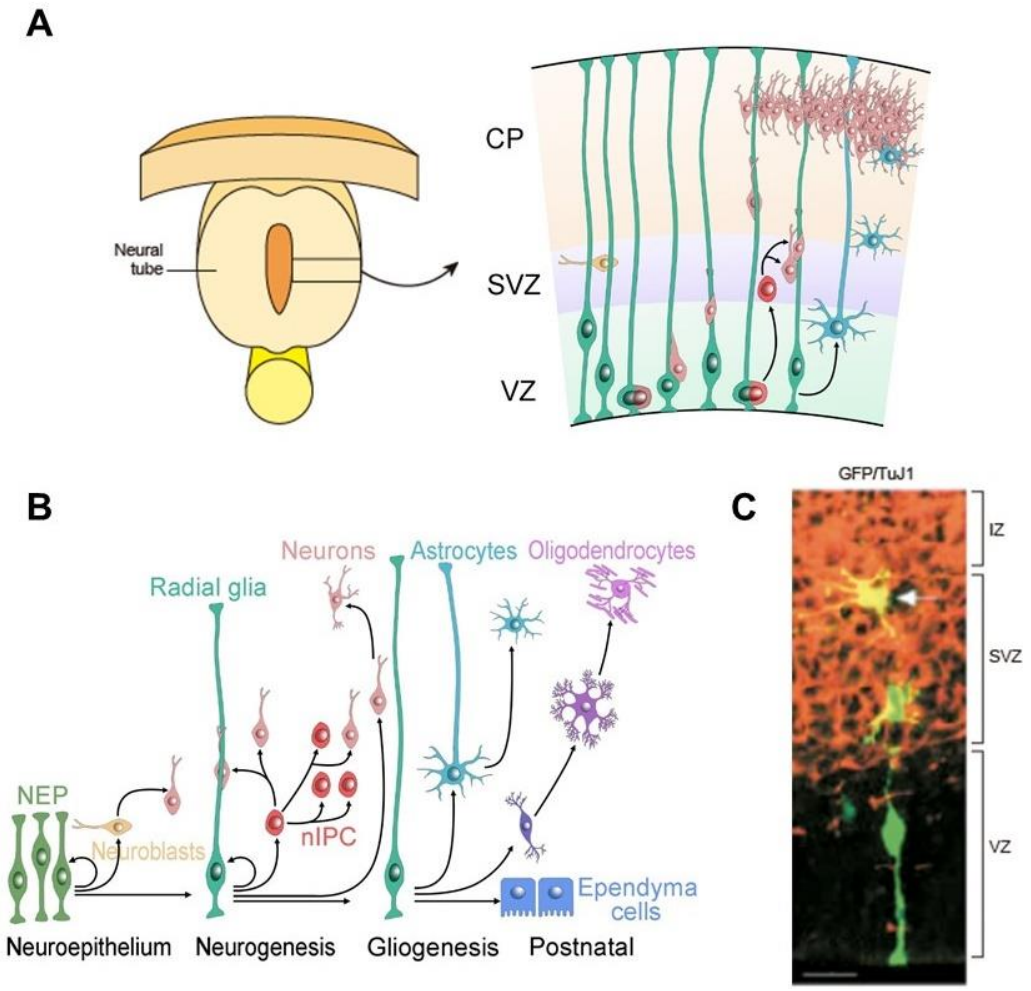

Fig. 1 – Radial glial progenitors (RGPs) in the developing neocortex. (A) In the early neocortex, radial glial cells (RGPs) span the wall of the neural tube. Later, RGPs division can give rise to several cell types that include neurons and glial cells. **(B)** Neuro epithelium precursors (originated from the primitive ectoderm) will differentiate into RGPs or other neuronal precursors, which will populate the neocortex, through symmetrical or asymmetrical divisions. **(C)** RGPs (GFP) divide at the ventricular zone to generate new neurons. VZ – Ventricular zone, SVZ – subventricular zone, IZ – intermediate zone and CP – cortical plate. Adapted from [1, 5] .

Newly born neurons, derived from RGPs or other precursors, migrate through a series of morphological stages towards the cortical plate (CP), where neurons become organized into six well-defined cortical layers [3]. Cells that migrate from the ventricular zone (VZ) and leave the cell cycle at early stages give rise to neurons that settle in the deepest layers of the cortex [6]. On the other hand, cells that exit cell cycle at later stages, migrate larger distances and become part of superficial layers of the cortex [6]. In the end, the majority of RGP cells mature and differentiate into astrocytes and oligodendrocytes, while some give rise to ependymocytes, a population of neural stem cells that avoided differentiation, in the adult brain [3, 6].

2. MOTOR PROTEINS ARE IMPORTANT FOR BRAIN DEVELOPMENT

Since all cells in the developing brain are very dynamic, their organelles need to be in constant movement. Intracellular transport of organelles, protein and mRNA complexes relies on molecular motor proteins that carry these cargoes along a cytoskeletal track. Three families of motor proteins are responsible for most of the active intracellular transport: Myosins, Kinesins and Dyneins. While Myosins use actin filaments as tracks, Kinesins and Dyneins walk on microtubules [7]. As microtubules (MTs) are polar structures, consisting of a plus end and a minus end, different motors have affinity to walk on a specific direction. Kinesins walk in the plus end-direction of the microtubules, to the cell periphery, while cytoplasmic Dyneins are minus end-directed microtubule motors that carry cargoes to the minus ends of microtubules, that are usually attached and stabilized to the centrosome or microtubule organizing center (MTOC) [8]. All motor proteins have domains for ATP hydrolysis to promote their movement and a tail domain that is responsible for binding to the different cargoes [7].

3. THE CELL CYCLE OF RADIAL GLIAL PROGENITORS

In order to progress through the cell cycle and divide, RGPs undertake a remarkable nuclei migration behavior known as interkinetic nuclear migration (INM) [3]. The periodic movement of the cell nucleus during INM occurs in phase with cell-cycle progression [9]. Once in G1, the nucleus is transported away from the ventricular surface (VS) to then undergo S-phase near the subventricular zone (SVZ). During G2, the nucleus migrates apically, back to the VS where it needs to be in order to enter mitosis **(Fig. 2) [10].** The purpose of INM is thought to be related with the need for clearing out nuclei from de VS after M-phase, allowing other RGPs to reach the apical surface and divide, and for the pseudostratified tissue organization of cells at the VZ, that allows epithelia to pack more RGPs in a limited area [3, 9]. In agreement with this, the VZ is one of the most proliferative regions in the early brain and participate in production of most of the neurons in the neocortex, as well as other regions, in the central nervous system (CNS) [11].

4. MOTOR PROTEINS DRIVE NUCLEAR MIGRATION

Although INM was first described several years ago by Sauer (1935) [9, 12], the underlying mechanism of this nuclear migration remained poorly understood until recently. Using *in utero* electroporation, Tsai *et al*., (2010) found that the migration of progenitor's nuclei during INM is powered by oppositely directed microtubule motors proteins, using a highly polarized (almost unidirectional) microtubule network arising from the centrosome at the VS. One of these motors is Kif1a (of the Kinesin-3 family) and the other is cytoplasmic Dynein-1, which is well known to act in intracellular transport of multiple organelles such as lysosomes and late endosomes in the cytoplasm of eukaryotes cells [13]. The activity of these motors during INM was also shown to be coupled with cell cycle progression [13]. Kif1a promotes basal migration of the nuclei, transporting them away from the VS during G1, while Dynein-1 is recruited to the nuclear envelope in G2, to exert pulling forces that will drive the nuclei back to the VS, where RGPs will then enter mitosis **(Fig. 2)** [3].

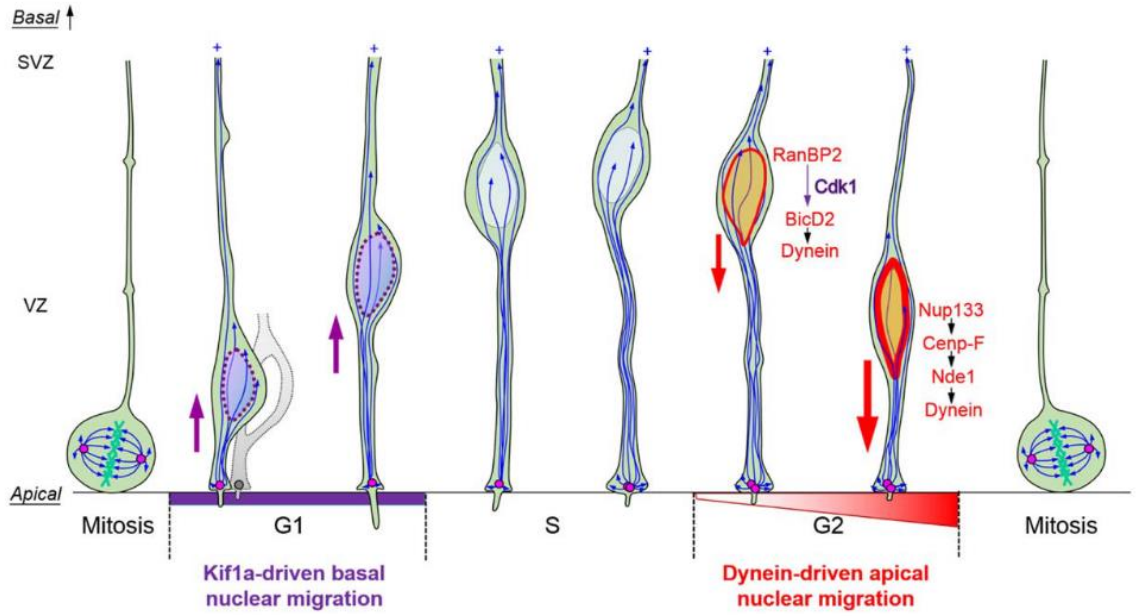

Fig. 2 – Interkinetic nuclear migration is a cell-cycle dependent mechanism that is promoted by motor proteins. Kif1a (purple) drives the basal migration of RGPs nuclei, where they remain during S-phase. In G2, nuclei are driven apically by cytoplasmic Dynein-1 (red), in order to position them in the VS, the only place they can divide. The two sequential pathways for Dynein recruitment to the nuclear envelope are also shown in red. RGPs microtubules network is highly polarized with the plus ends of microtubules located basally and minus ends located apically, near the VS. Adapted from [3].

4.1. Recruitment of Dynein-1 to the nuclear envelope

Given that nuclear movement in RGPs and succeeding mechanisms of neuronal migration are dependent on motor proteins, the recruitment of such motors to the nuclear envelope (NE) is tightly regulated by several proteins such as nucleoporins present at nuclear pores [10, 14].

In apical INM, Dynein-1 is recruited to the nuclear envelope, specifically during G2, via two pathways mediated by two different nucleoporins. In early G2, the nucleoporin RanBP2 binds the Dynein adaptor BicD2, which in turn recruits Dynein-1 to the NE. Later in G2, a second row of Dynein-1 recruitment uses the nucleoporin Nup133 that binds CENP-F, that will recruit NDE1/NDEL1, that associates directly with Dynein-1 **(Fig. 2)**. It is believed that the requirement for two pathways to recruit Dynein-1 is to generate greater forces, since, in apical INM, the nuclei must approach a very crowded ventricular surface of the brain [10, 14].

The NDE1/NDEL1 Dynein-1-recruitment pathway was shown to be critical in a late stage in the cell cycle – specifically during apical nuclear migration (INM) in G2 and finally at the G2-to-M transition [10, 15].

5. DYNEIN MOTORS

The Dynein motor protein was discovered more than 50 years ago by Ian Gibbons, as a protein that drives cilia/flagella movement in *Tetrahymena pyriformis* [16, 17]. It is named after the unit of force, dyne, transmitting the idea that this protein is involved in producing forces in cells. This Dynein was later found to be an axonemal Dynein.

In 1987, Paschal and Vallee identified another form of Dynein, involved in transport, using calf brain extracts [18]. This cytoplasmic Dynein-1 was later revealed to be the minus-end directed motor responsible for most of retrograde transport in cells.

Until now, nine major classes of Dynein heavy chains were found: two cytoplasmic and seven axonemal Dyneins. Axonemal Dyneins are responsible for movements of microtubules that drive the beating of cilia and flagella [19, 20] while, cytoplasmic

Dyneins are involved in intracellular transport of vesicles, proper localization of organelles, as well as several mitotic functions **(Fig. 3)** [19].

A common factor in all Dyneins is that they are large motor proteins, characterized by the presence of a highly conserved subunit called Heavy chain (a protein of approximately 500 kDa), which includes the motor domain and the AAA+ domains (ATPases associated with diverse activities) [19, 20].

Hereafter, I will focus on cytoplasmic Dyneins, their structure, function and regulators.

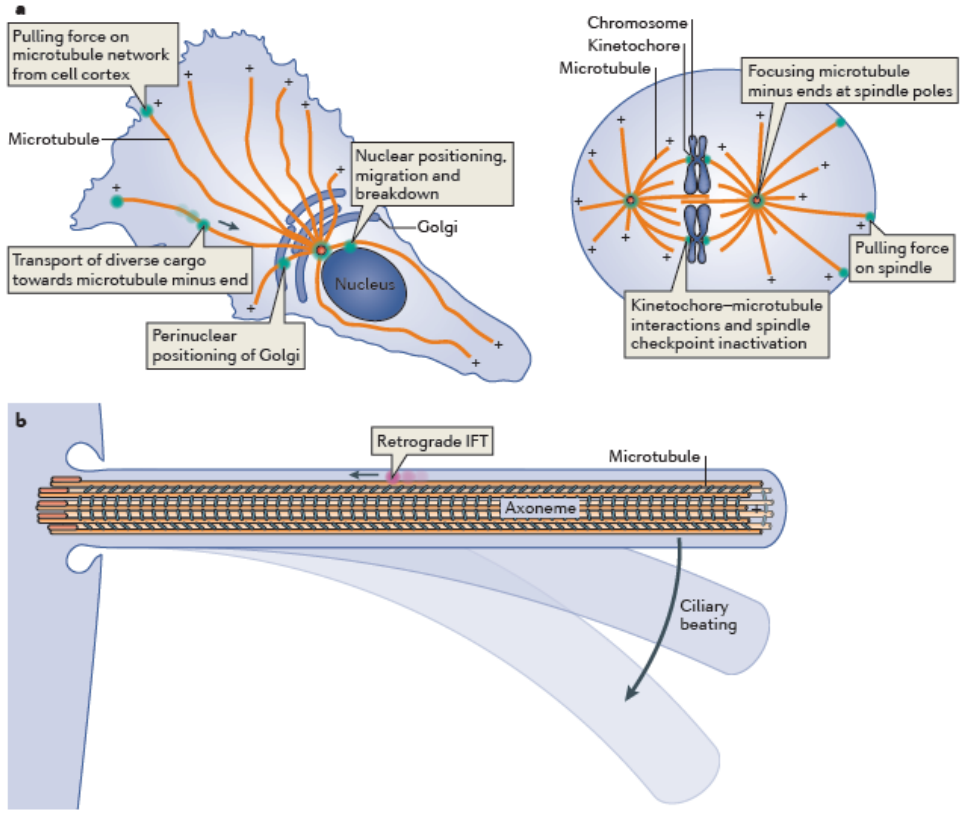

Fig. 3 – The motor protein Dynein diverse functions in cells. (a) Cytoplasmic Dynein-1 has several functions in interphase cells (e.g. neurons) and dividing cells. **(b)** In cilia, cytoplasmic Dynein-2 promotes retrograde transport along cilia microtubules, to promote cilia disassembly, while axonemal Dyneins power the beating of motile cilia. Adapted from [19].

5.1. Cytoplasmic Dynein-1

Cytoplasmic Dynein-1 is a 1.4 MDa motor protein complex, composed by a homodimer of two heavy chains and several accessory proteins. Each heavy chain contains a ring of six AAA+ ATPases, a microtubule-binding domain and a tail. The tail

of the Dynein heavy chain is important for the binding of regulatory subunits: intermediate chains (IC), light intermediate chains (LIC) and light chains (LC), that will promote Dynein complex assembly and binding to cargo adaptors **(Fig. 4)** [19, 21, 22].

Dynein-1 is responsible for several functions in cells (reviewed on [19, 21]):

- Retrograde cargo transport of endosomes, lysosomes, peroxisomes, mitochondria and Golgi, along microtubules.
- Exerting tension on cellular structures as the Golgi and nucleus.
- Assisting at several steps of mitosis (e.g. spindle positioning).
- Interkinetic nuclear migration in neural progenitor cells, as described earlier.

Dynein-1 is not processive on its own (processivity is the ability to walk for long distances and without falling out of microtubules); in order to be processive it needs to form a giant trimeric complex with a cargo adaptor such as BicD2 and Dynactin (a key Dynein-activating complex) **(Fig. 4)** [19].

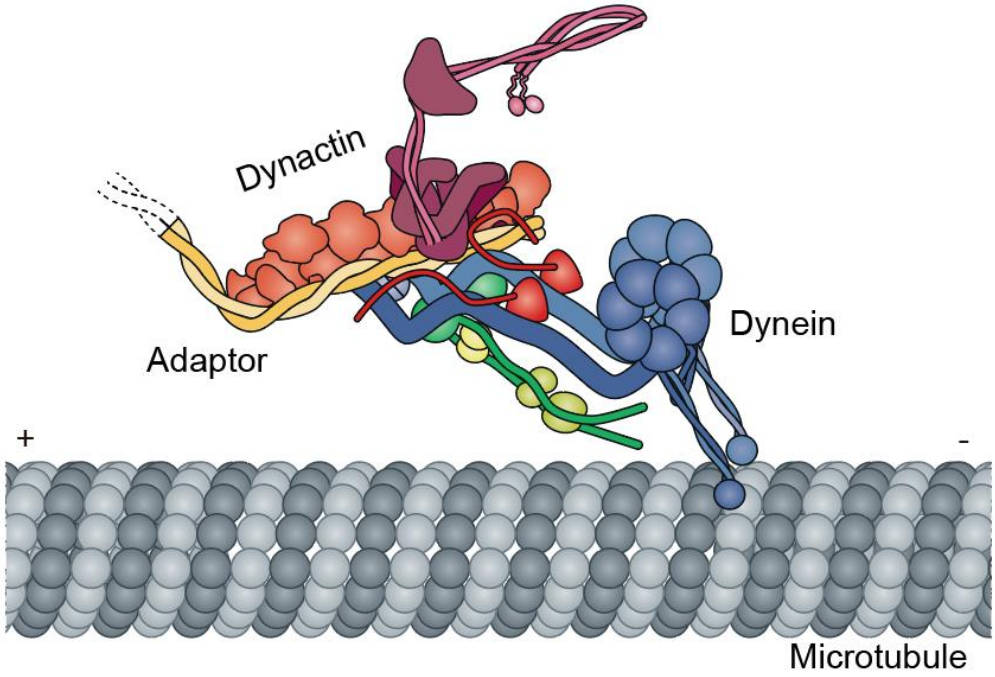

Fig. 4 – Cytoplasmic Dynein-1 trimeric complex. Dynein-1 has a motor domain (blue), that interacts with microtubules, and a tail domain, consisting of light intermediate chain (LIC) (red), intermediate chain (IC) (green) and light chains (LCs) (light green). The trimeric complex, formed by Dynein-1, a protein adaptor (yellow) and dynactin (purple), allows the complex to become processive on microtubules. (+) and (−) indicate microtubule polarity. Adapted from [21].

The Dynein-1 complex also interacts with other proteins that are critical to regulate its many functions. These include the Nuclear Distribution Element 1/Like 1(NDE1/L1; also known as NUDE/L) and lissencephaly-1 (LIS1; also known as NUDF) [19].

5.1.1. Dynein-1 regulators NDE1/NDEL1

NudE (NDE1) was firstly identified in *Aspergillus nidulans* in a screen for suppressors of NudF (LIS1) [23]. These proteins were characterized as “nud” because when mutated they affected nuclear distribution [23].

NDE1 in mammalian cell has a paralog, known as NDE1-like (NDEL1). These proteins are both ~39 kDa and share approximately 60% amino acid sequence identity (with 80% sequence similarity), which suggests that these two genes have evolved from a common ancestral gene [23, 24].

Both NDE1 and NDEL1 can bind both Dynein-1 IC and LIS1, through their coiled-coil regions, as shown in **Fig. 5**. The disorder region is responsible for binding to other interactors such as LC8, CENP-F and DISC1 [25].

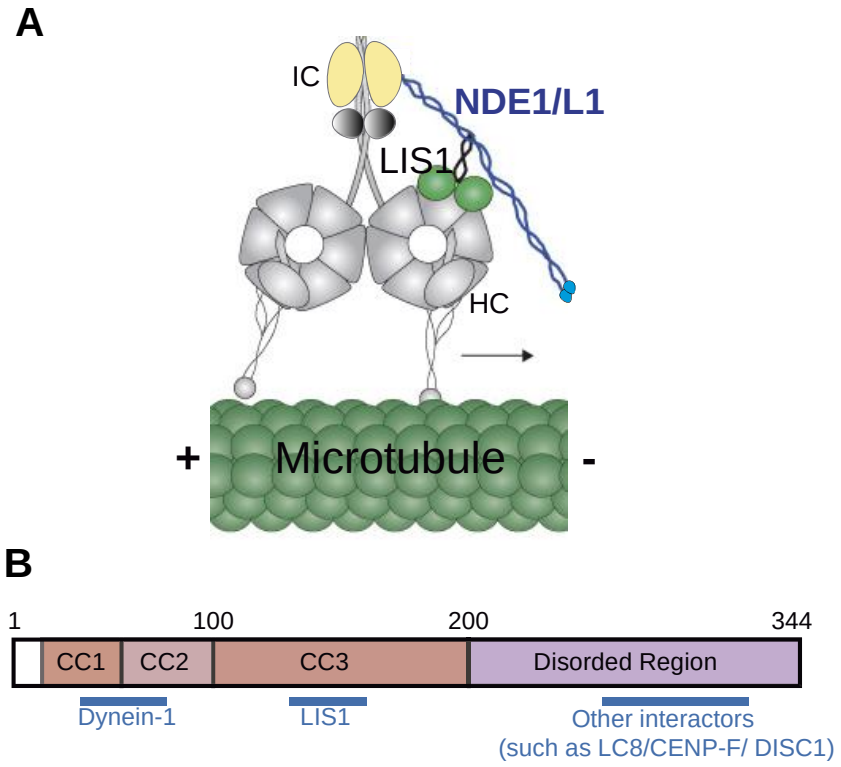

Fig. 5 – NDE1/L1 binds to LIS1 and Dynein-1, through coiled coils. (A) Schematic representation of NDE1-LIS1 complex binding to Dynein-1. At the same time, NDE1/L1 binds to

Dynein-1 IC and LIS1 binds to the Dynein-1 motor. **(B)** NDE1/L1 N-terminal region is composed of coiled coils, necessary for dimerization and binding both Dynein-1 IC and LIS1. The C-terminus of NDE1/L1 can bind other proteins, such as Dynein-1 and Dynein-2 light chain LC8.

Even though some NDE1 and NDEL1 functions overlap, these two proteins have some distinct and specific functions.

In order to distinguish the relevance of both proteins in development, knockout animal models were produced for both paralogs. Nde1 knockout mice showed a small brain, with the most dramatic reduction affecting the cerebral cortex, coherent with a microcephalic phenotype [26]. On the other hand, complete loss of Ndel1 resulted in early embryonic lethality, a phenotype comparable to the complete loss-of-function of Lis1 or the Dynein-1 heavy chain [27].

5.1.2. Dynein regulator LIS1

Dynein is also regulated by the NDE1/L1 cofactor LIS1. In mammals, LIS1 belongs to the non-catalytic subunit of the platelet-activating factor (PAF) acethylhydrolase (PAFAH). LIS1 non-enzymatic function is on the conserved pathway that regulates nuclear migration and like NDE1/L1, it was also discovered in the *A. nidulans* pathway [28].

LIS1 consists of two domains: N-terminal coiled-coil and seven WD-40 repeats [28].

LIS1 colocalizes with Dynein-1 at multiple sites in cells, including the kinetochores, centrosomes, mitotic cortex, and in migrating cells [29].

It was found that the complex Dynein-LIS1-NDE1 strongly enhances the ability of Dynein-1 to move along microtubules and be processive [30]. Recently, it was shown that LIS1 increases the rate of formation of the Dynein-dynactin-adaptor complex, as well as, processivity on microtubules. LIS1 was required for complex activation and assembly (by releasing Dynein from its auto-inhibited form), but not for sustaining maximal velocity, probably dissociating from moving complexes. It also stated that LIS1 also favors recruitment of two Dyneins to a single dynactin that results in increased velocity and force [31-33].

LIS1 was the first gene associated with a neurodevelopment pathology called lissencephaly. This pathology is characterized by problems in neuronal migration that lead to abnormal cortical thickness and reduced or absent gyri and sulci in the brain surface, leading to a smooth brain appearance [28].

LIS1 is an essential gene because loss of LIS1 results in embryonic lethality in a mouse model. Heterozygous mice mutants showed problems in neuronal migration as well as defects in progenitors and neurons morphology [34].

Using *in utero* electroporation, *LIS1* knockdown resulted in multiple problems in neurogenesis: from arrests in radial glial progenitor's cell cycle, decrease in the ability to give rise to neurons, problems in multipolar-bipolar neuronal differentiation stages, to impaired migration of neurons through all layers of the cortex [35].

5.2. Cytoplasmic Dynein-2 (cilia-specific)

Cilia are microtubule cell protrusions, nucleated from the mother centriole at the centrosome, that play many important functions in higher organisms. Cilia can be divided in motile cilia (also called flagella), essential for cell locomotion and nonmotile (sensory or primary cilia), that are required for receiving and transmitting signals [36].

Cilia assembly occurs at the centrosome and depends on a very specialized type of bi-directional transport of cargo, known as intraflagellar transport (IFT), mediated by two types of motors that move along the microtubule doublets of the ciliary axoneme. Anterograde IFT trafficking takes ciliary proteins from the base to the tip of the cilium to promote assembly/elongation and is driven by the microtubule motor Kinesin-2. On the other hand, retrograde IFT carries signaling molecules and the IFT machinery back to the base of the cilium and is performed by the Dynein-2 motor complex **(Fig. 6)** [37].

Cytoplasmic Dynein-2, better known as IFT-Dynein is also a retrograde motor, but it is restricted to cilia. The composition of the Dynein-2 motor complex is very similar to that of Dynein-1. As for Dynein-1, Dynein-2 is comprised of a heavy chain (HC) dimer and accessory proteins (a hetero dimer of intermediate chains IC), homodimer of light intermediate chains (LIC) and several light chains) [38]. In contrast to Dynein-1, very little is known regarding potential interactors and regulators of Dynein-2 function in IFT inside cilia. However, it was discovered that, Dynein-2 and Kinesin-2 are

integrated into long linear arrays called IFT “trains”. These IFT “trains” are multimeric protein complexes that contain two complexes of IFT particles (complex IFT-A and IFT-B) and several copies of the motors. IFT “trains” are, not only, the primary cargoes of Dynein-2 and Kinesin-2, but are also thought to function as cargo adaptors for the wide range of proteins that transit into and out of cilia during their functions **(Fig. 6)** [39].

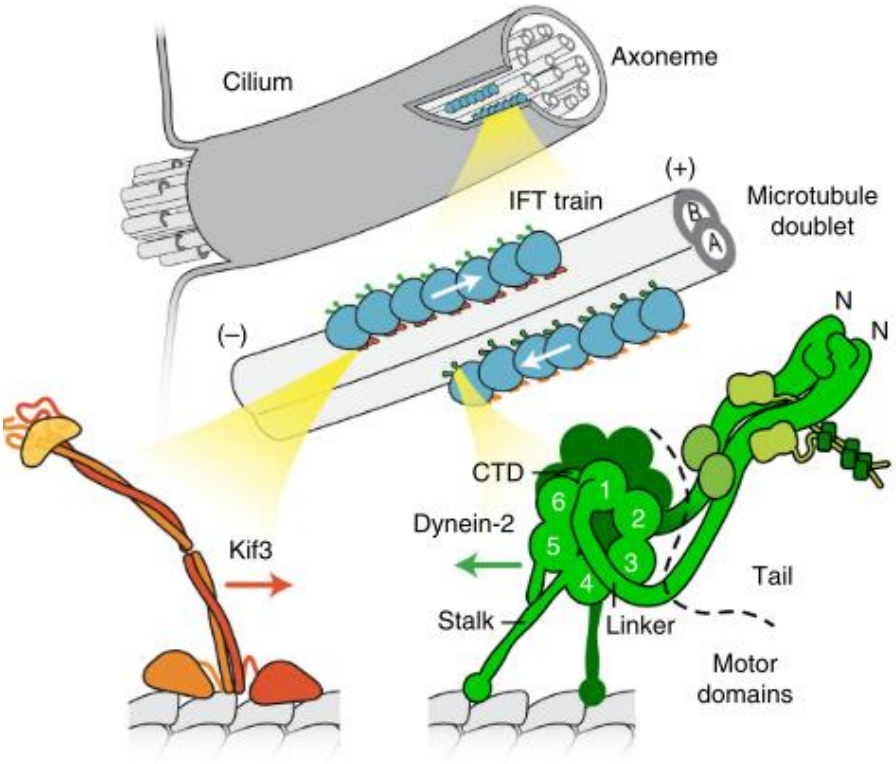

Fig. 6 – Transport in cilia occurs in IFT trains that move cargoes along microtubules. Kinesin-II family member Kif3 powers IFT transport towards the cilia tip, while Dynein-2 powers transport toward the cell body, the minus ends of microtubules. Dynein-2 (predicted structure in green) is a homodimer of two heavy chains, including the motor domain, and several subunits. Adapted from [40].

Several proteins are transported during IFT. One of the most important are tubulins, essential for cilia and axonemal cytoskeleton. IFT also transports important proteins for cilia-mediated signaling such as proteins involved in Hedgehog and Wnt signaling pathways [41].

Defects in cilia morphology or function, such as the ones originated from mutations in Dynein-2, can lead to a vast range of diseases, generally designated as ciliopathies [42]. One example was characterized by Taylor *et al.*, (2015) which found patients mutations in Dynein-2 light intermediate chain (*DYNC2LI1/* LIC), that were related with

short rib polydactyly syndromes (SRPSs), a ciliopathy that impairs the development of long bones accompanied by abnormalities in several organ systems [43].

6. *NDE1*-ASSOCIATED MICROCEPHALY

Disturbance in radial glial progenitors' proliferation, neurogenesis (ability to give rise to neurons), migration or cell function can result in a devastating brain developmental disorder known as microcephaly. Microcephaly is a rare lifelong condition characterized by a strong reduction in brain size and, unfortunately, in most of the cases, it results in several cognitive deficits and low life expectancy. This pathology can be caused by environmental or genetic causes (in an autosomal recessive pattern) [44].

Several genes have been associated with microcephaly and most of them are related with neurogenesis, specifically with centrosome or mitotic function [45]. More detailed information on microcephaly-associated genes is present on **Table S1** in supplementary data.

NDE1 was an early candidate gene for microcephaly, as studies had found that in homozygous *Nde1* null mice have severe decrease in brain size, with damage in the cerebral cortex, derived from problems in neurogenesis and cortical lamination [27]. Studies in humans later showed that inheritance of *NDE1* frameshift mutations and deletion of *NDE1* exons or locus where associated with severe cases of microcephaly [46, 47].

The severity of NDE1-associated microcephaly was believed to be caused by the participation of NDE1 in several aspects of neuronal progenitors' proliferation and subsequent neuronal migration.

In fact, Doobin *et al.*, (2016) found that depleting or changing the ratio between NDE1/NDEL1 can lead to three distinct arrests in the cell cycle of RGPs: (1) in regulation of primary cilia at the G1-to-S transition **(Fig. 7 – 1),** (2) during apical nuclear migration (INM) in G2 **(Fig. 7 – 2)** and finally (3) at the G2-to-M transition **(Fig. 7 – 3)** [15]. These findings highlighted the importance of NDE1 and its paralog NDEL1 in RGPs proliferation and brain development.

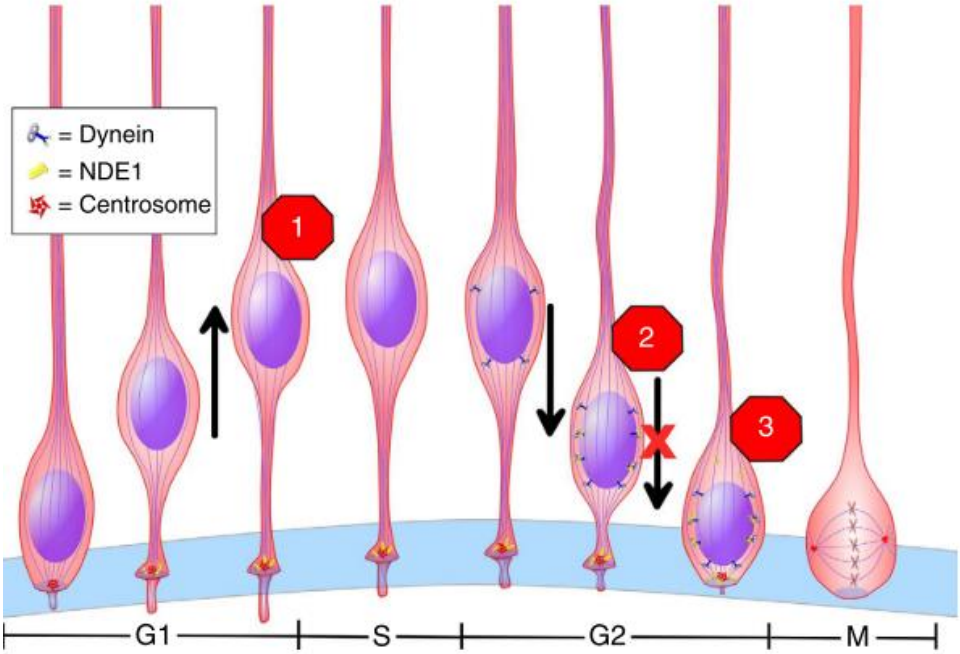

Fig. 7 – Depletion of NDE1 and NDEL1 in RGPs leads to arrests in 3 distinct stages of the cell cycle. 1 – G1-to-S transition; 2 – Apical nuclear transition during G2; 3 – G2-to-M transition. During INM, the centrosome is located at the RGPs end-feet (in the VS) and gives rise to a primary cilium in G1. The first arrest in the G1-to-S transition was found to be caused by problems in primary cilia resorption. Adapted from [15].

Knockdown of NDE1 had a clear effect on INM, leading to an arrest of the nuclei (approximately 10 µm away from the VS), without completion of the apical migration to the VS and, therefore, preventing RGPs from ever undergoing mitosis. In contrast, knockdown of the NDE1 paralog, NDEL1 had no phenotype on INM. [15].

Overexpression of NDEL1 rescued the arrest in apical INM caused by NDE1 depletion, demonstrating that higher levels of NDEL1 can compensate for NDE1 loss. However, cells ended up arresting after completing INM and before entering mitosis, uncovering a NDE1-specific role in mitotic entry [15].

Interestingly, combined knockdown of NDE1 and its paralog NDEL1 caused the earliest defect in the apical migration, with nuclei being arrested more than 30 µm from the ventricular surface, suggesting a synergistic function of the paralogs, in an earlier stage of the cell cycle. Indeed, staining with the G1 marker CyclinD1 revealed a potent G1 accumulation and therefore, a G1-to-S arrest [15]. This arrest was accompanied by a significant increase in primary cilia length, as assessed by co-electroporation with Arl13B-mCherry, a marker for primary cilia.

Interestingly, during INM and throughout the cell cycle, the centrosome stays at the apical end-foot of the RGP cell, at the ventricular surface of the brain **(Fig. 7)**. Here the mother (mature) centriole of the centrosome anchors to the apical plasma membrane to nucleate a primary cilium from the plasma membrane into the lateral ventricle where it may sense signals important for controlling cell proliferation [15, 48].

To test whether the G1-to-S arrest seen was cilium-dependent, Doobin *et al.*, (2016), co-depleted IFT172, which blocked anterograde IFT and inhibited ciliogenesis. The loss of the primary cilium rescued the G1-to-S arrest seen in NDE1/NDEL1 double knockdown [15].

These results showed that this particular arrest was cilium-dependent and suggested a role for NDE1/L1 in cilium regulation or signaling – perhaps through the regulation of the cilium-specific Dynein-2 in a similar manner to Dynein-1. In agreement with this hypothesis Kim *et al.,* (2011) found that Nde1 protein in mice localized to the cilium base and was required for its resorption, acting as a negative regulator of ciliary length. Also in this study, overexpression of NDE1 in human cells resulted in bulged and stumpy cilia, a characteristic phenotype of retrograde IFT defects and loss-of-function mutations in subunits of Dynein-2. [49].

Previous unpublished results from my supervisor show that NDE1/NDEL1 also localizes to the base of cilia, in RGPs endfeet **(Fig. 8)**. However, it remains to be determined how the G1 arrest phenotype arising from NDE1/NDEL1 depletion occurs. We hypothesize that NDE1/NDEL1 act by recruiting regulators of primary cilia IFT to the centrosome, directly regulating retrograde transport inside cilia and/or even by affecting cilia-mediated signaling.

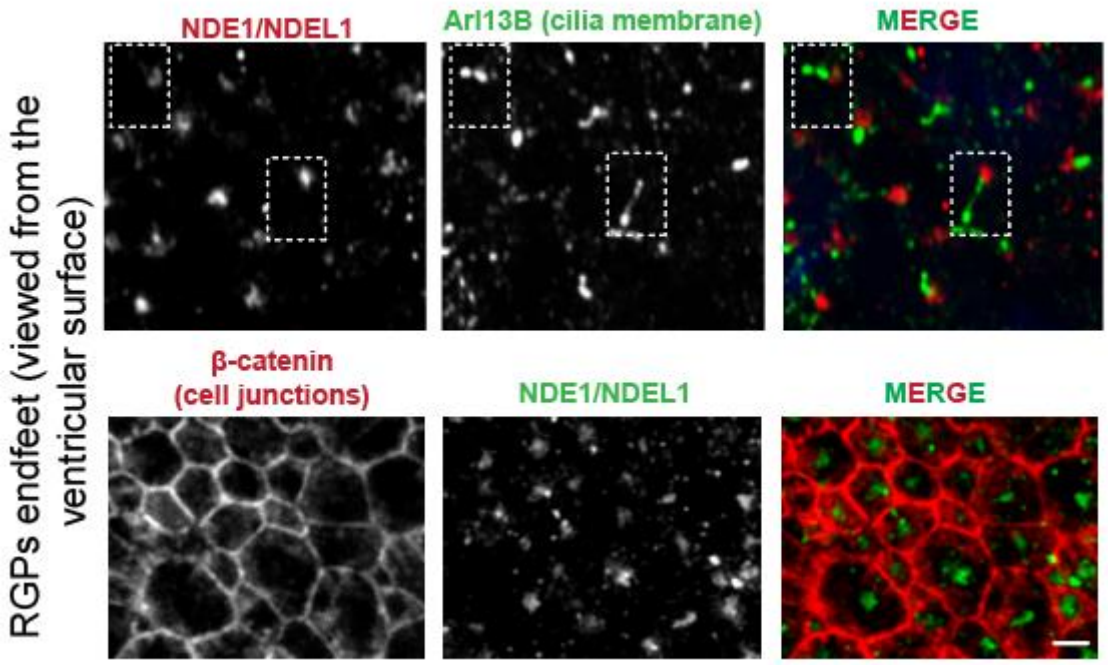

Fig. 8 – NDE1/NDEL1 also localizes to the centrosome, specifically to the base of cilia, in RGPs endfeet, at the ventricular surface. En-Face view imaging of embryonic E19 brain slices co-stained with a primary antibody against both NDE1 and NDEL1 and antibodies marking primary cilia or cell junctions at the RGPs endfeet. Scale bar = 2 µm.

In order to better dissect the molecular mechanisms involved in the regulation of the G1-to-S transition in RGPs, we made use of NDE1 point mutants that block specific interactions, performing *in utero* electroporation in rat embryos. We complemented our study with experiments using *Caernohabditis elegans* (*C. elegans*), a powerful system to study cilia formation and cilia-mediated signaling, as a way to assess how loss of NDE1/NDEL1 influence cilia's mechanisms.

AIM OF STUDY

The main goal of this project was to determine the contribution of NDE1 for Dynein-1 and Dynein-2 functions during neocortical development. This goal was divided into two sub aims using complementary model systems:

1. Determine which NDE1 roles in the cell cycle of RGPs require its interaction with Dynein-1 or LIS1. Using *in utero* electroporation of rat embryos, we aimed to express mutant forms of NDE1 unable to interact with LIS1 or with Dynein-1, already available in the lab. With this, we intended to achieve separation of functions of NDE1 and dissect its contributions at the G1-to-S transition.
2. Study if, in addition to functioning as a key regulator of Dynein-1, NDE1 is also important for Dynein-2 function in retrograde IFT. Using *Caenorhabditis elegans* we aimed to investigate a potential role for NUD-2 in cilia assembly, Dynein-2-mediated transport and cilia signaling functions.

MATERIAL AND METHODS

1. *IN UTERO* ELECTROPORATION TO STUDY NDE1 MUTANTS IN RGPS

1.1. Overview on *in utero* electroporation

In utero electroporation is a well stablished technique to study events of neural progenitor proliferation happening in the developing cortex [50]. Using this technique valuable data was discovered about how motor proteins and their regulators are involved in proliferation of neuronal progenitors, specifically in dissection of NDE1/L1 role in these events.

With this technique we can overexpress or silence genes in the developing rat brain, by injection and electroporation of DNA with positive electrodes directed to one of the brain ventricles of rat embryos. Because we are only electroporating a small fraction off all the cells, the rest of the brain will develop and maintain its normal functions and normal surroundings, which is a great advantage when working with proteins essential for survival.

1.2. Animals

I obtained accreditation from the Federation for Laboratory Animal Science Association (FELASA B) and was trained to successfully carry out in *utero* electroporation in gestating Wistar-Han rats. A total of twenty-three adult rats were included in this investigation. Animals were obtained from the i3S animal facilities and all procedures were conducted in agreement with institutional ethical guidelines (IBMC/i3S), the EU directive (2010/63/EU), Portuguese law (DL 113/2013), as well as FELASA recommendations. Our animal protocol also received the approval of the National Authority for Animal Health (DGAV; Lisbon, Portugal).

Animals were maintained under a 12 hour light/dark schedule with controlled temperature/air humidity and *ad libitum* access to food and water. Environment enrichment was used to ensure animal welfare.

1.3. *In utero* electroporation

E16 pregnant rats were anaesthetized using isoflurane and placed on a heating pad. Anesthesia induction was conducted at 5% isoflurane with 1 L/min O_2 flow. Once the animals lost the standing reflex, anesthesia maintenance was carried at 2% isoflurane and 0.2 L/min O_2 flow.

Pain control was provided by the administration of buprenorphine (concentration of 0.13 ml/100 g), via subcutaneous injection near the back of the neck. After anesthesia depth confirmation, the surgical site was prepared, first, by shaving the fur and cleaning the surgical site by alternating iodine and 70% ethanol sterile compresses, to ensure a proper antiseptic surgical site.

Sterility was maintained throughout the entire surgery by using sterile surgical gloves, sterile tools and a sterile drape over the incision site. The skin incision was made along the midline of the abdomen. Afterwards, an incision was made through the abdominal rectus muscle along the *linea alba*. The uterine horns were, then, carefully exposed from the peritoneal (abdominal) cavity and illuminated with a little flashlight, in order to visualize embryos and the two brain hemispheres.

1 µL of DNA **(Table 1)** combined with fast green was injected into the left lateral ventricle, using a needle made from a glass capillary tube (Drummond PCR pipettes 10 µL). Subsequently, using electrodes connected to an electroporator (BTX ECM 830 Electroporation Generator), five pulses of electrical current (50 V, 50 ms each, with 1 s intervals) were applied on the external wall of the uterine horn (as shown in **Fig. 9**). The uterus was returned to the abdominal cavity, the incision site and skin closed using 5/0 suture (Silk braided black, SMI). After awaking from the surgery, the animal was returned to its cage. HydroGel (Clear H_2O) was added to the animal's cage to help recovery and avoid dehydration. Buprenorphine was injected every 8–12 h for the first 48 hours and the animals were monitored every day post-surgery, following a red code monitoring scheme, until they were euthanized.

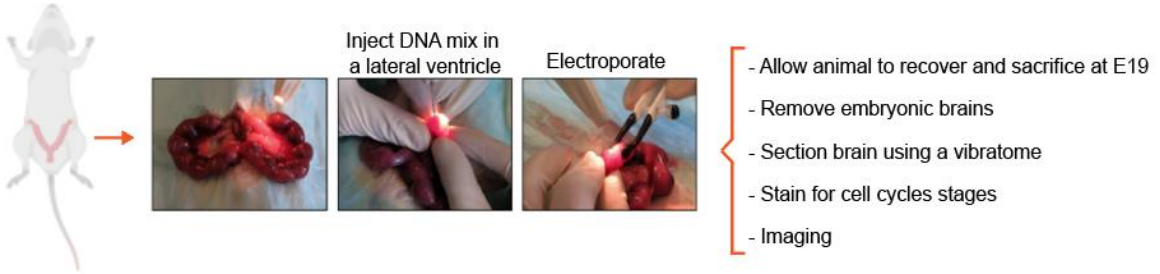

Fig. 9 – *In utero* electroporation workflow. At embryonic day E16, a survival surgery is performed in pregnant female rats. Uterine horns are carefully exposed, in order to inject a DNA mix in a lateral ventricle of the brain. Electrodes are placed on the surface of the uterus in a specific orientation, to allow electroporation of RGPs. Steps after sacrificing the mother are shown on the right.

1.4. DNA constructs used for electroporation

NDE1 and NDEL1 shRNA vectors used in this project were previously validated in Doobin *et al.*, (2016) [15]. shRNAs were contained in a pRetro-U6G vector (Cellogenetics, MD, USA), which co-expressed GFP and the shRNA sequences. The target sequence for NDE1 used was 5′- GCG TTT GAA TCA AGC CAT TGA -3′ and the target sequence for NDEL1 was 5′- GAT GGT GAA GAT ATA CCG GAT -3′. shRNA knockdown efficiency is shown in **Fig. 10**.

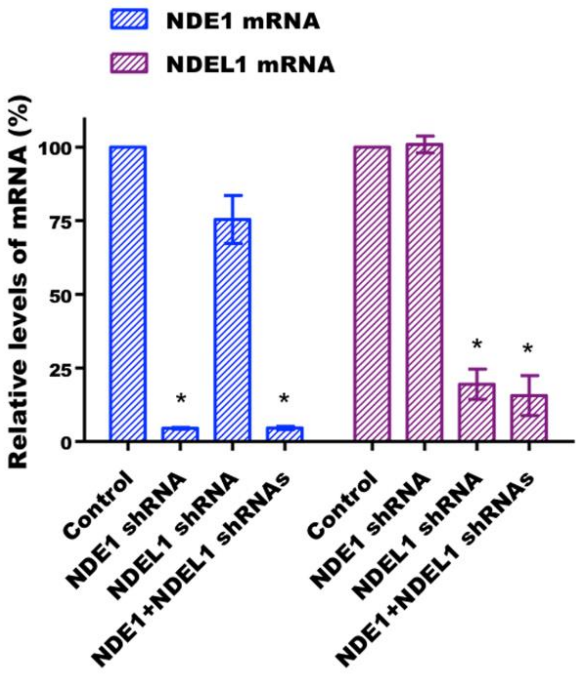

Fig. 10 – shRNA knockdown efficiency. mRNA levels from C6 glioma cells were used to measure the efficiency and specificity of NDE1 and NDEL1 shRNAs by qRT-PCR. These data were obtained

by Tiago Dantas (whom authorized their inclusion in this thesis), and were published in Doobin *et al.*, (2016) [15].

The NDE1 rescue construct expresses mouse NDE1 (92% identity to rat NDE1), which had been shown to rescue rat NDE1/L1 depletion [15], cloned in a pCAG-IRES-DsRed2 vector (driven by CAG promoter, consisting of the cytomegalovirus (CMV) enhancer fused to the chicken beta-actin promoter and rabbit beta-Globin splice acceptor site). This construct has five silent point mutations in the target sequence (5′- A CGC TTA AAC CAG GCC ATT GA -3′) so that its expression was resistant to the NDE1/NDEL1 shRNAs.

Two novel constructs, cloned prior to this project, both based on pCAG-IRES-DsRed2 mNDE1 were tested: one carrying mutations that abolish its interaction with Dynein-1 IC (E47A, E51A) and another unable to bind LIS-1 (E118A, R126A, R129A) (REF).

As negative control empty vectors were used (pCAG-IRES-DsRed2 and pCAG-IRES-GFP).

Table 1 – Constructs used for *in utero* electroporation.

Plasmid	Stock concentration (µg/µl)	Volume used in a 10 ul DNA mix (µl)
NDE1 shRNA pRetro-GFP	3.3	4
NDEL1 shRNA pRetro-GFP	3.3	4
pCAG-IRES-DsRed2	2.7	2
pCAG-IRES-GFP	2.8	3.5
pCAG-IRES-DsRed2-mNDE1	2.4	2
pCAG-IRES-DsRed2-mNDE1 119.127.130	2.7	2

pCAG-IRES-DsRed2-mNDE1 47.51	2.4	2

1.5. Preparation of brain slices

Four days after surgery at E19, pregnant rats were euthanized using a CO_2 machine. CO_2 euthanasia was carried out using the following guidelines: CO_2 pressure set to 2-3 bar, induction time of 7 minutes with progressive amounts of CO_2 and a dwell time of 2 minutes.

Embryos were then excised from the uterus of the sacrificed animal and the embryonic brains were quickly dissected. Brains were fixed in 4% paraformaldehyde (PFA), diluted in PBS, overnight at 4ºC. 24-48 hours after fixation, PFA was replaced with PBS. Following fixation, brains were embedded in 4% agarose (in PBS) and sliced with a vibratome (Leica VT1000 S), to prepare 100 µm thickness coronal slices.

1.6. Immunostaining

Successfully electroporated brain slices were selected after screening for fluorescence at a dissecting scope and moved into a 24 well dish. First, they were incubated in blocking/permeabilizing solution (0.3% Triton X-100 in PBS and 2% normal donkey serum) for 1 hour, at room temperature (RT).

Slices were then incubated with primary antibodies, diluted in blocking solution, overnight at 4ºC. After washing slices three times with PBS, they were incubated with secondary antibodies (and DAPI), also diluted in blocking solution, for 4 hours at RT. Antibodies used in this study were rabbit polyclonal against CyclinD1 (Thermo Scientific, RM-9104, 1:200 dilution), donkey fluorophore-conjugated secondary antibodies (cy5) (Jackson Labs, 1:600 dilution) and DAPI (4’,6-diamidino-2-phenylindole, Thermo Scientific, 62248, 1:10 000 dilution).

Sections were mounted on glass slides (SuperFrost Plus Adhesion slides, Thermo Scientific) with mounting media (20 mM TRIS pH=8, 0.5% N-propyl gallate and 90% glycerol).

1.7. Imaging and data analysis

Images were acquired with a Zeiss Axio Observer microscope equipped with an Orca Flash 4.0 camera (Hamamatsu) and controlled by ZEN software (Zeiss). Brain sections were imaged using a 63x oil immersion objective (N.A. 1.4 Plan-Apochromat objective) or a 10x air objective (N.A. 0.3 EC Plan-Neofluar objective). All images were processed in ZEN software (Zeiss) to perform image deconvolution (deconvolution defaults, parameter: good, medium speed (fast iterative)).

Brain images were also acquired with a laser scanning confocal microscope Leica TCS SP5 II, composed of 4 lasers (Diode 405 nm, Ar 458, 476, 488, 496, 514 nm, DPSS561 561nm and HeNe 633nm) and controlled by LAS AF (Leica Microsystems, Germany). In this microscope, brain sections were imaged using a 63x 1.30 N.A. glycerol immersion objective or a 10x 0.40 N.A. air objective.

All images were analyzed using ImageJ/Fiji software (NIH, Bethesda, Maryland, USA). RGPs soma distance was measured by tracing a segmented line from the ventricular surface (RGPs endfeet) to the bottom of the cells soma.

2. *CAERNOHABDITIS ELEGANS* AS A MODEL TO STUDY CILIA FUNCTION

2.1. General overview

C. elegans is a small (~1 millimeter in adult form), non-pathogenic nematode of the *Rhabditidae* family. *C. elegans* life cycle is extremely fast, which allows a single hermaphrodite worm to successfully populate one entire plate in a week. There are several additional advantages of using this animal model: worms can be frozen at -80ºC to maintain a permanent strain stock, and defrost when needed; worms can be

kept at three different temperatures: 25ºC, 20ºC and 16ºC, which makes it possible to control the rate of growth of these animals (**Fig. 11**), and their genome can be easily manipulated by CRISPR-Cas9 [51].

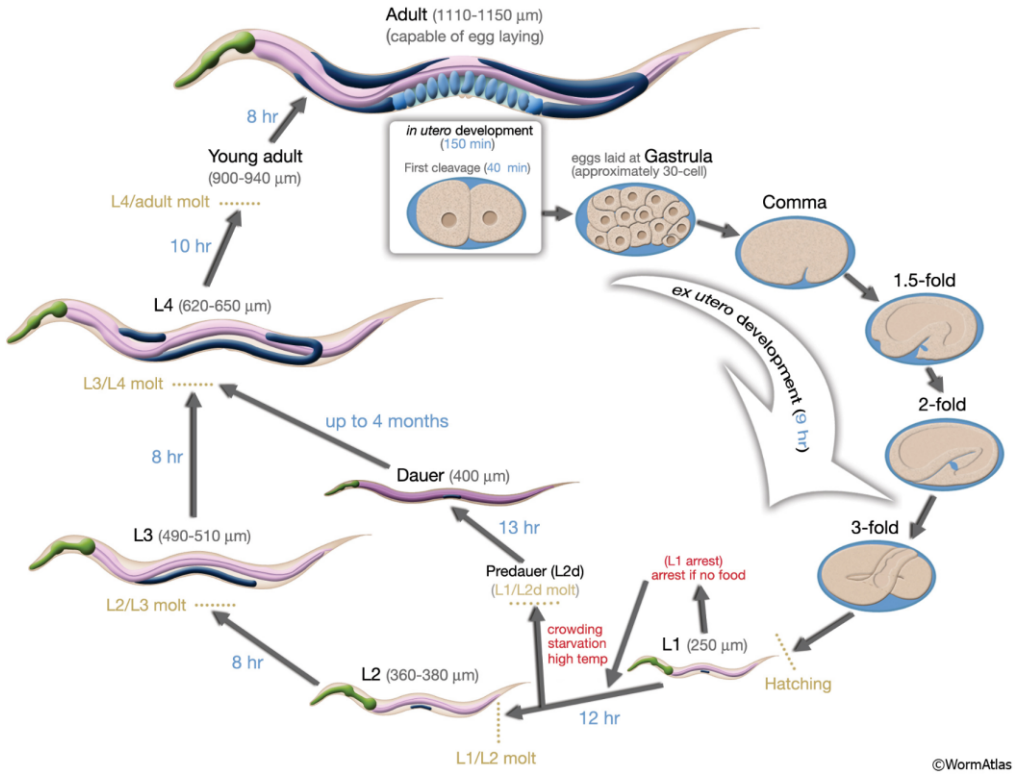

Fig. 11 – *C. elegans* life cycle. *C. elegans* worms have a rapid life cycle that consists of *in utero* development, four larval stages (L1 to L4) and adult stage. In *C. elegans*, an alternative life cycle pathway – "dauer" – can be activated at L1, in case of unfavorable environment conditions like crowding, starvation and high temperatures. Adapted from WormAtlas.

2.2. *C. elegans* sensory cilia

C. elegans can exist as hermaphrodites or as males (frequency of <0.2%). This was the first animal organism to have its entire nervous system mapped. Hermaphrodites develop 302 neurons, whereas males have 383 neurons in their nervous system. Of the 302 neurons in the hermaphrodite, 60 are ciliated at the endings of their dendrites, while males have 48 additional ciliated neurons [51]. The major types of ciliated sensory neurons are amphid and phasmid sensory neurons **(Fig. 12)**. Additional sensory neurons are inner/outer labial neurons, cephalic neurons and other disperse neurons [52]. Most of these sensory neurons have key functions in worms which are related with simple behaviors, like food exploration, noxious

substance avoidance, chemoattraction, dauer entry, mechanosensory and mating behavior [52].

Since only sensory neurons have cilia and these are not essential for survival, this model system is particularly appealing for this project. In addition, knockout and knock-in strains of NUD-2 (the NDE1 ortholog in worms) and Dynein-1/-2 subunits were available in the lab **(Table 2)** providing very useful tools to study the importance of NUD-2 (NDE1) in cilia formation, IFT, and functions of cilia in sensory neurons.

.

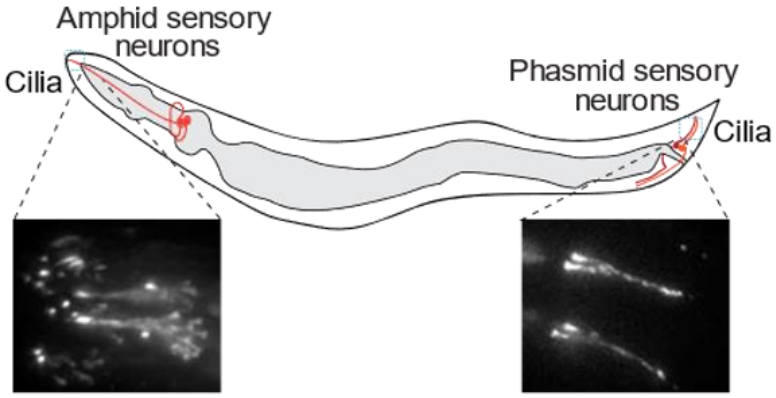

Fig. 12 – *C. elegans* sensory cilia. In *C. elegans*, cilia are restricted to the dendrites of sensory neurons and are mainly presented in the amphid (head) and phasmid (tail) sensory neurons. Sensory cilia can be visualized by labeling molecules responsible for transport inside cilia, IFT. In this case, cilia were visualized by GFP-labeling of IFT74, one subunit of the IFT trains.

Amphid sensory neurons (ASE, ASG, ASH, ASI, ASJ, ASK, ADF, ADL, AWA, AWB, AWC and AFD) have their somas/cell bodies near the pharynx of worm, and their axons are associated with the nerve ring. Their dendrites are extended to the anterior end of the worm and terminate with sensory cilia (some cilia are exposed to the environment) [52].Phasmid sensory neurons (PHA and PHB) are located in the tail of the worms, exposed to the external environment [52].

Table 2 – *C. elegans* orthologs of important genes for this study.

Human	*C. elegans*	Encodes
NDE1/NDEL1	*nud-2* (Chromosome I)	Known Dynein-1 regulators with additional functions in cilia
IFT74	*ift-74* (Chromosome II)	Subunit of IFT complex B
DYNC2LI1/LIC3	*xbx-1* (Chromosome V)	Light intermediate chain of Dynein-2
DYNC2H1/DHC2	*che-3* (Chromosome I)	Heavy chain of Dynein-2
WDR60	*c27f2.1/wdr-60* (Chromosome III)	Intermediate chain of Dynein-2 (unpublished)

2.3. Worm maintenance

Worms were maintained at 20ºC or 16ºC, on Nematode Growth Medium (NGM) agar petri plates seeded with *Escherichia coli* strain OP50. This bacteria strain has limited and slower growth in NGM plates, which is an advantage for worm's visualization and for worm mating. Instructions for the preparation of NGM can be assessed on WormMethods available on Wormbook.

All strains used in this work and their respective genotype are listed on **Table 3**.

In order to maintain strain stocks, worms were transferred from an old plate to a new plate either by picking individual worms with a platinum wire coupled to a Kolle handle or by cutting a chunk of agar and placing it on a new plate.

When plates were contaminated with other bacteria or fungi, *C. elegans* cultures were decontaminated by bleaching adult gravid hermaphrodites, with a bleaching protocol (5% solution of sodium hypochlorite in 0.5 M NaOH). Since only eggs were able to survive this treatment, it was possible to obtain an uncontaminated offspring in a new plate.

For indefinite storage, *C. elegans* strains were frozen at -80°C. Starved worms' plates (containing mostly L1 stage larvae) were washed with S-basal (100 mM NaCl,

50 mM Potassium Phosphate, pH 6 and 5 mg/L Cholesterol in EtOH) and collected in a 15 ml falcon tube. Tubes were spun down at 600 g for 3 min, and the supernatant was removed. An equal volume of S-basal and worm freezing media (Glycerol 30% (v/v), 50 mM Potassium Phosphate, pH 6, 100 mM NaCl) was used to resuspend worms. 1 ml of worm suspension was added to Corning cryovials, that were, afterwards, stored on CoolCell containers (Mr Frosty), at -80ºC.

Table 3 – List of strains that were used in this study (name, genotype and source). Some strains were provided by the Caenorhabditis Genetics Center (CGC), a repository for *C. elegans* strains, funded by NIH Office of Research Infrastructure Programs.

	Strain	***Genotype***	***Source***
Wild-type and markers	N2	WT (ancestral N2 Bristol)	CGC
	GOU2162	*che-3(cas443[gfp::che-3]) I; xbx-1(cas502[xbx-1::tagRFP::3xFlag]) V*	CGC
	GOU2362	*ift-74(cas499[ift-74::gfp]) II*	CGC
	GCP97	*nud-2(ok949) I; unc-119(ed3) III; prtSi37[pRG200;Pnud-2::nud2::mCherry::StrepTagII::nud-2 3'UTR; cb-unc-119(+)] II*	GC lab
	TD9	*nud-2(ok949) I; unc-119(ed3) III; prtSi37[pRG200;Pnud-2::nud2::mCherry::StrepTagII::nud-2 3'UTR; cb-unc-119(+)] II; che-3(cas443[gfp::che-3]) I*	Made in this study
	TD47	*wdr-60-linker::3xFlag::GFP, III* (outcrossed 6x)	Made by Diogo Rodrigues and Carla Abreu
XBX-1 mutants	JT11069	*xbx-1(ok279) V*	CGC
	TD21	*xbx-1(ok279) V; ift-74(cas499[ift-74::gfp]) II*	Made in this study
	OE3002	*him-8 (e1489) IV; xbx-1 (ok279) V*	CGC

NUD-2 mutants	GCP66	*R11A5.2(ok949) I outcrossed 6x with N2*	GC lab
	TD61	*R11A5.2(ok949) I; him-8 (e1489) IV*	Made in this study
	TD4	*R11A5.2(ok949) I; ift-74(cas499[ift-74::gfp]) II*	Made in this study
	TD6	*R11A5.2(ok949) I; xbx-1(cas502[xbx-1::tagRFP::3xFlag]) V*	Made in this study
	TD53	*R11A5.2(ok949) I* outcrossed 6x with N2*; wdr-60-linker::3xFlag::GFP, III*	Made in this study

2.4. Genetic crosses

New strains are normally generated by crossing two or more already existing strains. In this case, Δ*nud-2* mutant strains were crossed with ciliary markers strains, to allow proper visualization of cilia.

Strain screening was achieved by performing worm lysis and PCR. A single worm was picked into a PCR tube lid containing 10 µL of lysis mix. To prepare the lysis mix, 5 µL of 20 mg/ml Proteinase K was added to 95 µL of 1 x PCR lysis buffer (10 mM Tris pH 8, 50 mM KCl and 1.5 mM $MgCl_2$), for a 10 worms' reaction. PCR tubes were, first, incubated at 65ºC for 90 minutes and then, at 95ºC for 15 minutes, as a way of inactivating Proteinase K.

Each single worm PCR reaction contained: 4 µL ddH_2O, 6.25 µL NZYTaq II 2x Green Master Mix (Nzytech), 0.63 µL forward and reverse primers (10 µM) and 1 µL of worm lysis. PCR conditions are described on **Table 4**.

Table 4 – PCR conditions to assess the genotype of new strains. * Annealing temperature was optimized for each primer set and calculated based on the primer T_m. It was used a touchdown PCR approach in which the initial annealing temperature is higher than the optimal T_m of the primers and is gradually reduced over sequential cycles.

Cycle step	***Temperature***	***Time***	***Cycles***
Initial denaturation	95ºC	2 min	1
Denaturation	94ºC	30 s	25-37
Annealing	*	30 s	
Extension	72ºC	30 s/kb	
Final extension	72ºC	5 min	1

PCR primers, used in this study, are described on **Table 5**, as well as their target genes.

PCR products were loaded to a 1% agarose gel, containing 2 µL GreenSafe Premium (Nzytech) per 100 mL of 1x TAE buffer (stock 50x TAE buffer contained 2 M of Tris base, 1 M glacial acetic acid, and 50 mM EDTA, pH 8). DNA ladder, NZYDNA Ladder II (Nzytech), was also loaded to the gel, as a way of accurately determine the molecular weight of PCR products. The agarose gel was run at 115 V for 50 minutes and, then, visualized on Gel Doc XR (Biorad).

Table 5 – Primers used in this study and their target genes.

Primer	***Sequence (5' → 3')***	***Annealing Tm (ºC)***	***Screen***
oTD3 (FW)	GTTCGACGCCTCGTTGAGAA	60-50	*xbx-1::rfp* knock-in
oTD4 (RV)	CACCAATACAAGTCTAAGCTAG		
oTD54 (FW)	ACAGGTGGAGTGTATTTAATGAG	60-50	*gfp::che-3* knock-in

oTD55 (RV)	GGAATCCAGAAATATCTCAAGTG		
oRG866 (FW)	CAGGCGGCATTATACGTTTT	59-49	*nud-2* deletion
oRG867 (RV)	AATGTTAAGCCCGTGTCGTT		
oTD5 (FW)	CACGAGTATGACTCACAAGGAG	60-50	*ift-74::gfp* knock-in
oTD6 (RV)	CGGAAAGGGTGCTTCATACTTG		
oRG287 (FW)	GACATTTGAGAATGGCATTGA	57-47	Mos II insertion
oRG288 (RV)	TTTACAAGGACTTGGATAAATTGG		
oTD41 (RV)	CAAATGCCACAAGATACGGAC	61-51	*wdr60::gfp* knock-in
oTD42 (FW)	TCATAACATACTGGGATTTGGG		

2.5. Dye filling assays

Lipophilic fluorescent dye DiI was used to perform dye filling assay as a way of testing cilia integrity and staining the morphology of ciliated sensory neurons.

Briefly, young adult worms were washed with M9 buffer and incubated in a 6 ug/ml solution of fluorescent dye (DiI; 1,1'-dioctadecyl-3,3,30,30,-tetramethylindo-carbocyanine perchlorate, Sigma) (stock 8 mg/ml) in M9 buffer at 20ºC. After one hour of incubation, worms were washed two times in M9 and transferred to NGM seeded plates. After 30 min, worms were examined for dye uptake by fluorescent microscopy (schematic in **Fig. 13**).

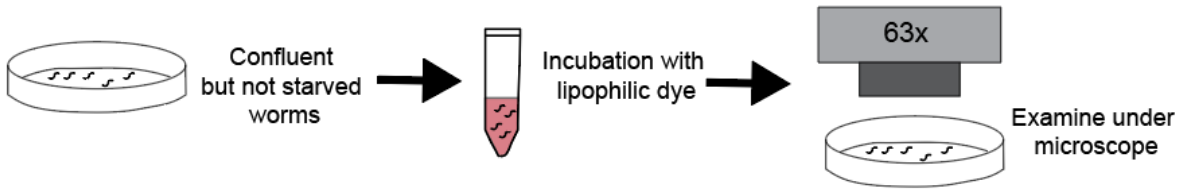

Fig. 13 – Dye filling assay workflow.

A total of at least 50 worms of each strain were examined in three independent experiments. In each session positive and negative controls were used.

2.6. Microscopy

2.6.1. Preparing slides

One drop of 5% agarose was placed on a glass slide and quickly covered with a second slide to provide even thickness. The top slide was removed after some minutes and microscopy pad was ready for use.

2.6.2. Mounting worms

Young adult *C. elegans* hermaphrodites were transferred to a drop of levamisole (5 mmol/L levamisole in M9 buffer), to anesthetize and paralyze the worms. After that, the coverslip was mounted to the 5% agarose pads.

2.6.3. Fixed fluorescence microscopy

Images were acquired with a Zeiss Axio Observer microscope equipped with an Orca Flash 4.0 camera (Hamamatsu) and controlled by ZEN software (Zeiss). Images were acquired with a 63x oil immersion objective (N.A. 1.4 Plan-Apochromat objective). The microscope was allocated in a temperature-controlled room, at 20ºC.

All images were processed in ZEN software (Zeiss) to perform image deconvolution (deconvolution defaults, parameter: simple).

2.6.4. Live imaging

Live imaging was carried out on an Andor Revolution XD (Andor Technology) microscope, with IQ 2 software (ANDOR Technology, UK) and equipped with Solid State Laser 488 nm (50 mW) and Solid State Laser 561 nm (50 mW). Live imaging was performed using a PLAPON 60x N.A 1.42 oil immersion objective (pixel size: 0.1385 µm) in a temperature-controlled room, at 20ºC. Images were taken at a frame-rate of 330 ms and each slice was imaged for no longer than an hour.

2.6.5. Transmission electron microscopy (TEM)

Processing of worms for TEM was performed by i3S facility HEMS – Histology and Electron Microscopy. Briefly, adult worms were fixed in freshly prepared 2.5% glutaraldehyde and 2% paraformaldehyde in 0.1 M sodium cacodylate at RT. Then, samples were washed in 0.1 M sodium cacodylate buffer - 3 times 5 min each. Samples were post-fixed in 2% osmium tetroxide in 0.1 M sodium cacodylate (2 hrs at RT – O/N at 4ºC), and then washed in water - 3x 5min each. Samples were incubated with 1% Uranyl acetate during 30 min at RT - O/N at 4ºC and washed in water. After dehydration (with gradual increases of ethanol and 3x Propylene oxide (PO)), tissues were included in resin, starting with 3 parts PO : 1 part EPON, 1:1, 1:3 and only EPON, during 48 hrs at 60ºC. Samples were then sectioned with a glass knife (starting from the worms' nose) to achieve semifine sections. Selected sections were then cut with a diamond knife and placed on EM grids, that were stained with heavy metals.

2.7. Behavioral assays

2.7.1. Mating assays

16 hours before the beginning of the mating assay, males from controls or mutant strains were separated to new plates, to avoid mating with other worms before the assay.

Six males (control or mutant strains) and six L4 hermaphrodites (N2 WT) were placed on a mating plate (NGM seeded plate with a central 1-cm spot of bacteria). After 24 hours on the mating plate, hermaphrodites were singled out to NGM plates (one hermaphrodite per plate) and allowed to lay eggs for 16 hours (as shown in **Fig. 14**). After two days, plates were checked for males and total progeny was counted. Three repetitions were performed.

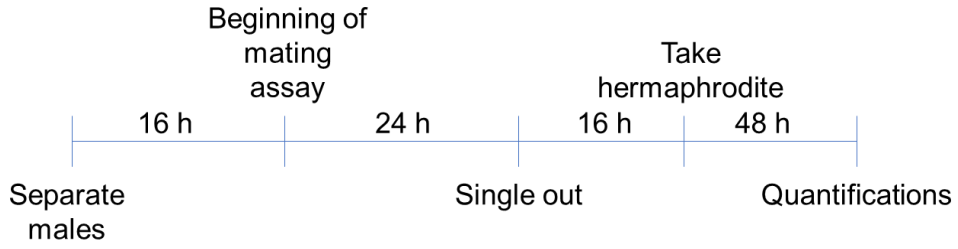

Fig. 14 – Mating assay workflow.

2.7.2. Chemotaxis assays

Chemotaxis assays were carried out by Dr. Neide Vieira (ICVS-Braga). Chemotaxis assays were performed with synchronous adult worm at 20 °C. Worms were first washed in CTX buffer (1 mM $CaCl_2$, 1 mM $MgSO_4$, 5 mM KH_2PO_4 pH 6.0). The assay started with placing worms in middle of the plate, giving the same distance to the attractants, diacetyl (DA, 1% in absolute ethanol) or isoamyl alcohol (IA, 10% in absolute ethanol) and vehicle (absolute ethanol) regions. NaN3 (1 M) was added to the attractant and vehicle regions of the plates, to prevent the worms from moving and allow quantification. After 1 h, it was calculated the chemotaxis index having in account the worm's distribution in the assay plate.

2.8. Data analysis and statistics

All measurements and signal intensities were obtained using ImageJ/Fiji. IFT74 average velocity was obtained with the Image J/Fiji plugin KymoAnalyzer. KymoAnalyzer is an open-source ImageJ package of macros that can be used for calculation of transport parameters by tracing segments in neurons or cilia and generating kymographs [53].

Values in figures and text are reported as mean ± standard deviation (SD). Statistical analyses were performed with GraphPad Prism 7.0 software. The type of statistical analysis performed is indicated in the figure legends. Differences were considered significant at P values below 0.05 (*$p<0.05$, **$p<0.01$, ***$p<0.001$ and ****$p<0.0001$).

RESULTS

1. *IN UTERO* ELECTROPORATION OF NDE1 MUTANTS TO SEPARATE FUNCTIONS

1.1. Double knockdown of NDE1 and NDEL1 leads to a significant increase in the CyclinD1 positive cells

In order to further dissect NDE1 functions during brain development we first had to establish and optimize *in utero* electroporation at i3S.

We performed control surgeries to improve the ratio of survival and to attempt to replicate the NDE1/L1 double knockdown phenotypes already published, so that we could then test the overexpression of new NDE1 point mutants.

Using Wistar pregnant female rats, we performed *in utero* electroporation of E16 embryos, using GFP alone or the combination of shRNA against NDE1 and NDEL1. At E19, we sacrificed the mother, and the embryos to dissect their brains. After brain fixation, we sectioned and screened for slices expressing GFP. Positive brain slides were stained with CyclinD1 (accumulates in cells in G1) and imaged in an epifluorescence and a confocal microscope.

Using a 10x lens, it was possible to observe RGPs due to the GFP alone or coupled to the shRNAs in the electroporation phase **(Fig. 15)**. In addition, it was possible to observe strong GFP signal in neurons in the upper layers of the cortex, as neurons derive from RGPs and therefore, when RGPs differentiate into neurons, they inherit the GFP signal.

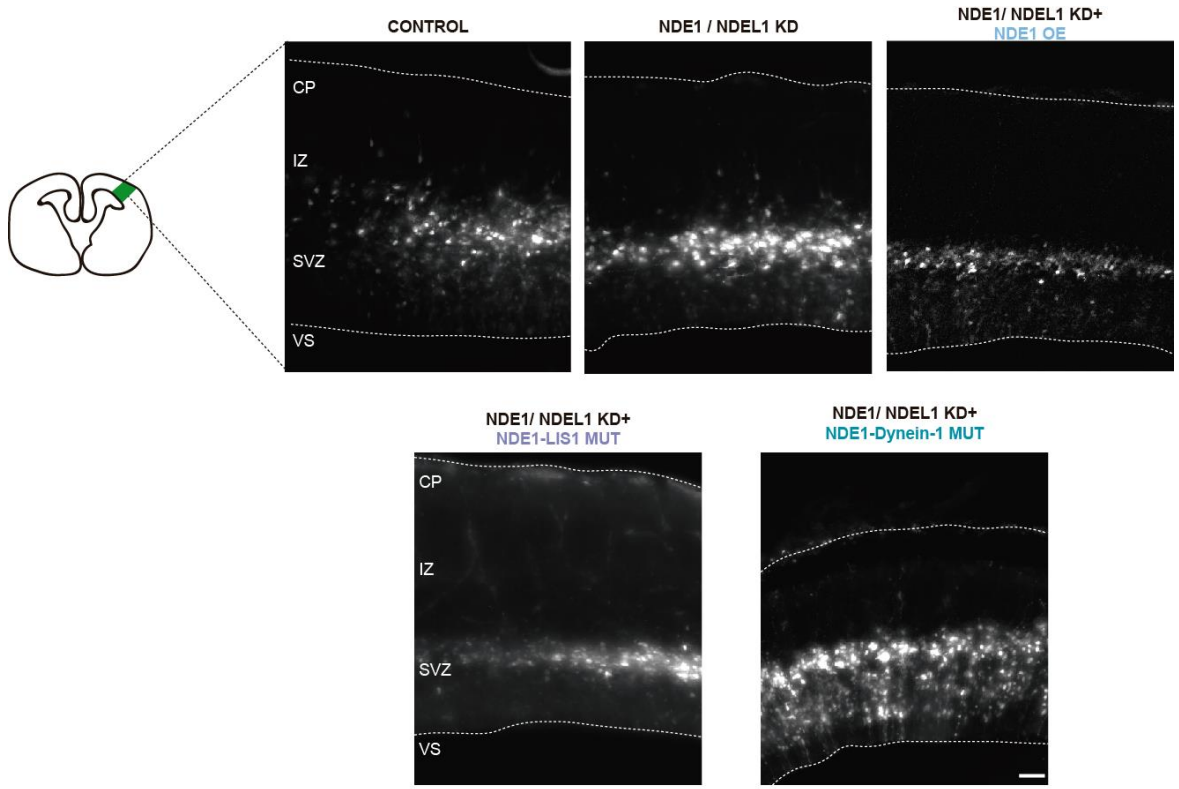

Fig. 15 – Visualization of RGPs (near the VS) and neurons by expression of GFP alone (control) or GFP coupled to shRNAs (double knockdown of NDE1 and NDEL1). Overexpression with novel constructs NDE1-LIS1 mutant (MUT) and NDE1-Dynein-1 MUT was carried out on the double knockdown background (mutants were expressed with DsRed – data not shown). VS – Ventricular surface, SVZ – subventricular surface, IZ – intermediate zone and CP – cortical plate. Scale bar = 50 μm.

Knowing that in rodents RGPs are the only progenitors at the ventricular surface (VS) that have two processes, we used 60x image to quantify the number of RGPs present in the brain slice based on the presence of basal and apical processes, and an endfoot connected to the VS. For the electroporated RGPs we verified if they were positive for CyclinD1 staining, and if so, we designated them as CyclinD1+ RGPs. We also measured the distance from their nuclei to the VS using Image J **(Fig. 17)**.

When analyzing the effects of double knockdown of NDE1 and NDEL1, we noted a considerable increase in the CyclinD1 positive cells, pointing out that RGPs were accumulating in G1, and not proceeding in the cell cycle (52.7% and 37.1%, for the double knockdown and control, respectively). We also found a wider distribution of RGPs after measuring the distances from the ventricular surface to the RGPs nuclei (44.53 μm and 25.21 μm, for the double knockdown and control, respectively) **(Fig.**

17). Both sets of results were in accordance with what was reported in Doobin *et al.*, (2016).

Following this, we tried to rescue these phenotypes by overexpression of full length RNAi-resistant mNDE1 NDE1 in an IRES vector, co-expressing DsRed, an approach we will use later with our NDE1 point mutants. Overexpression of mNDE1 resulted in an amelioration of the G1 accumulation caused by the NDE1/L1 depletion, reducing the CyclinD1 index (44.5%) and resulted in a partial rescue of RGPs distribution (34.28 μm), even though it still did not completely reestablished the normal distribution of RGPs **(Fig. 17)**. These results were also in accordance with the previous study.

1.2. NDE1/L1 rescue experiments with NDE1-LIS1 and NDE1-Dynein-1 mutants

To determine which NDE1 functions are independent of LIS1 or Dynein-1, and better understand which mechanisms that might be regulating the G1-to-S transition, we performed rescue experiments by *in utero* electroporation, using already made constructs of mutated NDE1 forms that cannot bind its cofactor LIS1 or Dynein-1.

In order to abolish the interaction between NDE1 and LIS1, we used an already prepared NDE1 construct consisting of three single point mutations E118A, R126A and R129A, in the CC3 of NDE1. It is well established that these mutations prevent the binding of NDE1 to LIS1, without interfering with NDE1 binding to Dynein-1 [25, 54, 55]. On the other hand, to prevent binding of NDE1 to Dynein-1 we used a NDE1 construct containing two single point mutations E47A and E51A, that exclusively prevents the binding of NDE1 to Dynein-1 IC [25, 54]. A schematic of mouse NDE1 and NDE1 construct mutations is present on **Fig. 16**.

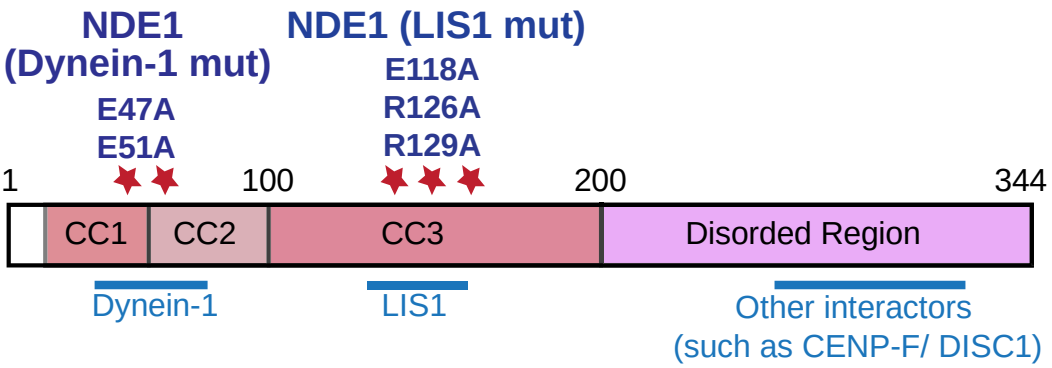

Fig. 16 – Mouse NDE1 schematic and construct mutation. A construct with two point mutations (E47A and E51A) and a construct with three point mutations (E118A, R126A and R129A) was used to selectively impair NDE1 binding to Dynein-1 or LIS1.

Overexpression of NDE1 unable to bind LIS1 did not rescue the potent G1 accumulation observed in the double knockdown of NDE1 and NDEL1. In fact, we noticed an even higher increase in CyclinD1 positive cells (64.5%) when compared to the double knockdowns (52.7%), as shown in **Fig. 17B**. Also, overexpression with NDE1-LIS1 MUT resulted in RGPs arrest farther away from the VS (34.27 μm) when compared to controls (25.21 μm), but the distribution of RGPs for the double knockdown of NDE1 and NDEL1 remained higher (44.53 μm) **(Fig. 17C)**.

On the other hand, overexpression of NDE1-Dynein-1 MUT had a 42.1% CyclinD1+ RGPs in the total number of RGPs electroporated. This result suggests that mutant was capable of rescuing the G1 accumulation observed in the double knockdown of NDE1 and NDEL1, to values similar to the control and full length NDE1 overexpression (**Fig. 17B)**. Also, in this mutant, RGPs were less dispersed than in the double knockdown, but localized more distant (33.25 μm) than controls, perhaps due to failure in INM in G2 **(Fig. 17C)**.

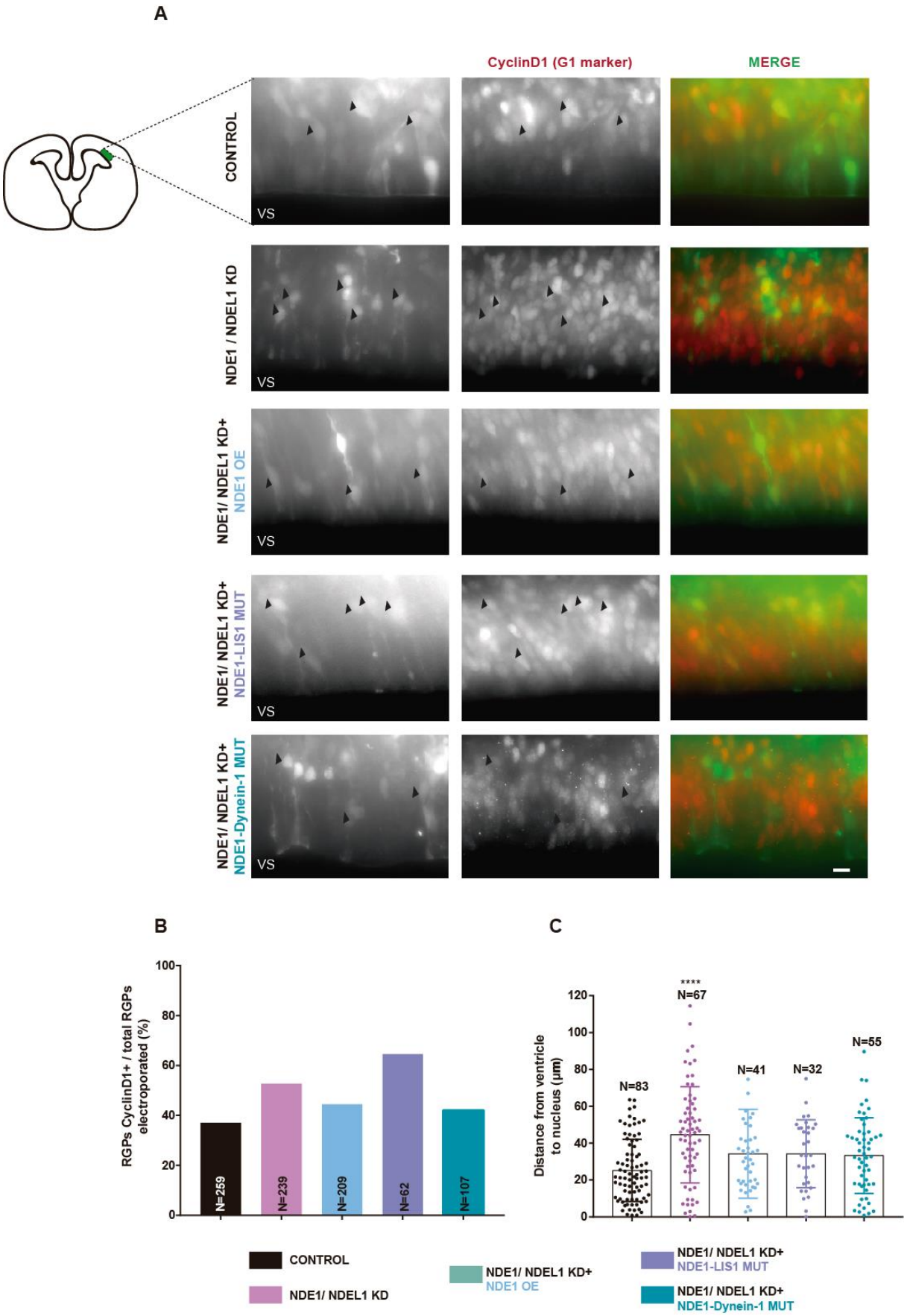

Fig. 17 – NDE1-LIS1 MUT and NDE1-Dynein-1 MUT rescue experiments. (A) Representative images of the VS of electroporated brains for all conditions, stained with CyclinD1, a G1 marker. Overexpression of NDE1-LIS1 NDE1-Dynein-1 mutant results in a potent accumulation of RGPs in

G1, whereas overexpression of mutant mostly rescues the double knockdown G1 accumulation phenotype. Scale bar = 5 μm. Arrowheads represent CyclinD1 positive RGPs **(B)** Quantifications of the number of CyclinD1+ RGPs over the total number of RGPs electroporated, for all conditions. **(C)** Measurements of distances between the bottom of the nucleus and the apical endfoot at the VS (apical process length), in all conditions. It is of note that for the quantification of RGPs distribution, we only measured RGPs that we were able to visualize the apical process. Statistical test for the distance measurements: One-way ANOVA (nonparametric), multiple comparisons to control. OE – overexpression, KD – knockdown, MUT – mutant. ****p<0.0001.

As different brains and surgeries gave very different amount of electroporated cells we decided to avoid premature statistical analyzes in the quantification of CyclinD1+ RGPs. We plan to image more RGPs for the different conditions to have a better idea of the effects on RGPs distribution and for each experiment set to have similar N.

2. STUDY OF CILIA FUNCTIONS IN THE ABSENCE OF NUD-2 (THE *C. ELEGANS* ORTHOLOG OF NDE1/L1)

2.1. NUD-2 is not an essential protein in *C. elegans*

Contrarily to what happens in mammals/humans, in which NDE1 is needed for most of Dynein-1 functions, colleagues in the Gassmann lab showed that, the NDE1/L1 ortholog in *C. elegans*, NUD-2 is dispensable for survival and several Dynein functions [56]. Since knockout of NUD-2 leads to viable worms and progeny, we took advantage of the already existing *nud-2* null allele *ok949* (*Δnud-2*) to study the effect of loss of NUD-2 in cilia formation and cilia-related processes like IFT and cilia-mediated signaling.

2.2. NUD-2 can localize near/inside *C. elegans* cilia

In the context of Dynein-1, Simões *et al.*, (2018), found that the transgene NUD-2::mCherry inserted in the *Δnud-2*, was expressed in *C. elegans* one cell embryo and localized to the mitotic spindle, a known place for Dynein action [56]. As described at

the introduction, in RGPs, NDE1/L1 localizes to the RGPs endfeet, specifically at the base of primary cilia.

Because we wanted to examine if NUD-2 was also localizing to cilia in *C. elegans*, we crossed this strain (Mos chromosome II insertion NUD-2::mCherry strain) with a strain carrying GFP::CHE-3 (N' terminus GFP knockin in Dynein-2 Heavy chain), a cilia marker and key component of Dynein-2.

NUD-2::mCherry has the tendency to aggregate, so it was very difficult to analyze their relative position to cilia. In **Fig. 18**, we have represented one case in which we could localize NUD-2::mCherry near the cilia marked with GFP::CHE-3.

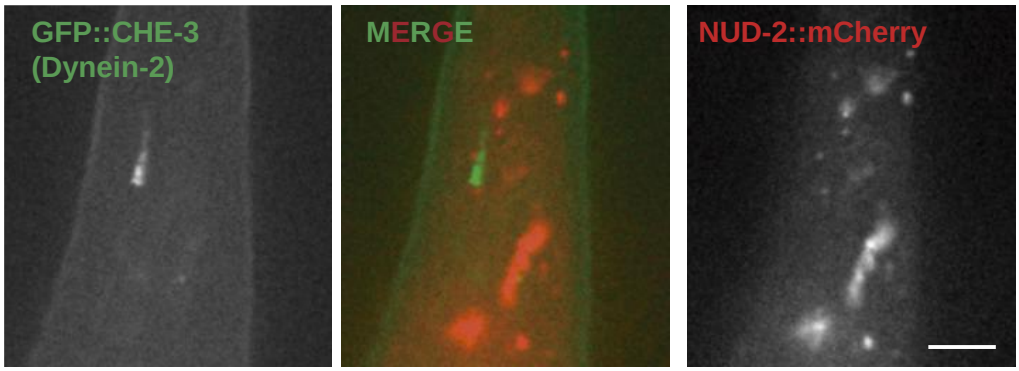

Fig. 18 – NUD-2::mCherry localization. NUD-2::mCherry can be localized, in some cases, near the cilia base. Scale bar = 5 µm. Single plane image.

We also saw NUD-2::mCherry near the cilia and at the cilia base in some other cases, but with high variability.

2.3. Morphology of sensory neurons in *Δnud-2*

First, we started by analyzing the integrity of cilia and the morphology of the ciliated sensory neurons in the *Δnud-2* mutant strain, by performing a classic dye filling assay [57]. It is believed that dye uptake occurs via the ciliated endings of sensory neurons that are exposed to the surrounding environment, staining those neurons with a fluorescent dye that can be visualized using fluorescence microscopy. Therefore, when cilia fail to assemble, the respective sensory neurons fail to uptake dye.

We performed this assay with three strains: N2 WT (positive control for dye uptake), *Δnud-2* and *Δxbx-1* (Dynein-2 LIC null mutant, known to fail to uptake dye [58]).

The fluorescent dye is normally uptaken by six amphid neurons (ASI, ADL, ASK, AWB, ASH and ASJ) in the head and the two phasmid neurons (PHA and PHB) in the tail, that have the cilia extending through the cuticle and in contact with the external environment. As expected, worms from the WT strain were able to uptake the fluorescent dye that filled those sensory neurons dendrites and somas. In contrast, *Δxbx-1* worms with abnormal cilia did not uptake dye into their sensory neurons, as previously described [58]. The only fluorescent signal detected was in the digestive tract, probably because some of these worms ingested some amount of dye during the incubation period. Mutant worms from the *Δnud-2* strain were able to uptake the fluorescent dye in a similar pattern as the WT control suggesting that cilia can be formed in *Δnud-2* sensory neurons **(Fig. 19)**.

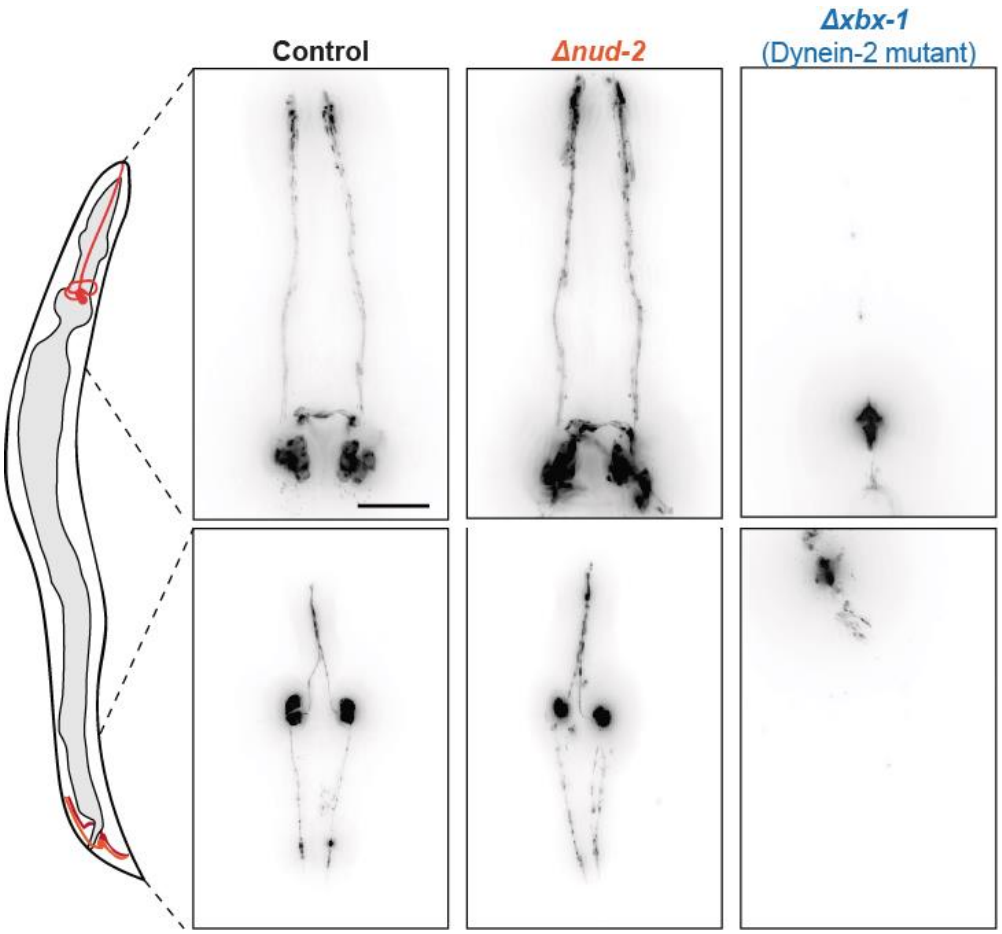

Fig. 19 – Dye filling profile in sensory neurons of control, *Δnud-2* and *Δxbx-1* worms. Top – amphid sensory neurons. Bottom – phasmid sensory neurons. Scale bar = 10 µm.

Taking advantage that *Δnud-2* neurons were stained by the dye we were able to see that the morphology of sensory neurons was mostly normal in *Δnud-2* worms.

2.4. Loss of NUD-2 does not interfere with cilia length but seems to alter distribution of IFT particles

Because the lack of a dye filling mutant phenotype does not imply proper cilium structure or function, we sought to analyze more directly if loss of NUD-2 has any effects on cilia assembly and intraflagellar transport (IFT) in phasmid sensory neurons. For this, we crossed the *Δnud-2* strain with an IFT74::GFP knock-in strain (a cilia marker that is a component of the IFT complex B).

In *C. elegans*, IFT presents some particularities: two kinesins are needed for anterograde transport: in the middle segment of cilia both heterotrimeric kinesin-II and homodimeric OSM-3-kinesin, bind IFT complexes and transport cargoes and Dynein-2 to the tip. In the distal segment, OSM-3-kinesin is the only kinesin responsible for anterograde transport. Dynein-2 is responsible for the retrograde transport, transporting back to the cilia base several cilia molecules **(Fig. 20) [52]**.

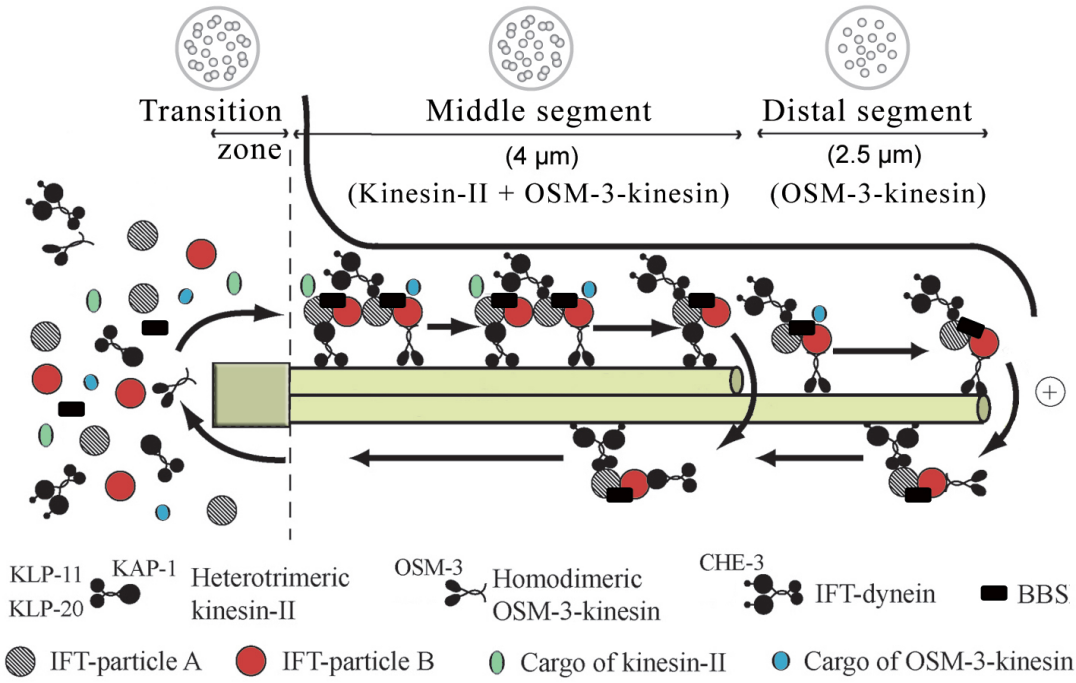

Fig. 20 – IFT in *C. elegans*. Two kinesins and Dynein-2 are the known molecular motors involved in IFT. Adapted from [52].

Using the image processing software Image J, we could measure sensory cilia length by tracing a line on each cilium marked with IFT74::GFP **(Fig. 21A)**. We did not observe any significant differences when comparing cilia length in control and Δ*nud-2 worms* (mean of 8.44 ± 1.22 µm and 8.19 ± 0.75 µm, respectively). In contrast, cilia length was very decreased in *Δxbx-1* worms (3.56 ± 0.77 µm), which was already expected, since this strain is a null of Dynein-2 LIC, a subunit essential for the stabilization of Dynein-2, as well as for IFT transport [43, 58] **(Fig. 21B)**.

Next, we started by analyzing the total distribution IFT74::GFP inside cilia and we noticed a decrease in total IFT74::GFP in cilia **(Fig. 21C)**. In order to detect potential defects in ciliary transport, we also analyzed the IFT74::GFP signal distribution along cilia. To do this analysis, we divided the cilia in equal intervals, and measured the mean normalized intensity using Image J. IFT74::GFP signal distribution was altered in the Δ*nud-2* mutant, more specifically at the base of cilia (in the first ~1.6 µm) and at the tip (in the last ~1.6 µm). In this mutant, IFT74::GFP signal increased in the first 20% of cilia, whereas, it decreased at the tip, in the last 20% of cilia, when compared with controls **(Fig. 21D)**.

Because of these alterations in IFT74::GFP signal distribution, we decided to study the kinetics of this particle transport in cilia. For this, we performed live imaging of IFT74::GFP, in a confocal spinning disk microscope. Then, we analyzed particle kinetics, in this case, IFT average velocity, using KymoAnalyzer software, a package of Image J plugins [53]. Examples of kymographs generated with KymoAnalyzer, for the control and Δ*nud-2*, are shown in **Fig. 21E**. From these kymographs, we traced lines for particles undergoing anterograde and retrograde transport and we could obtain the particles average velocity.

Loss of Δ*nud-2* does not alter anterograde IFT velocity, but it seems to significantly affect retrograde IFT velocity (for control velocity was 0,609 ± 0,287 µm/s and for mutant was 0,393 ± 0,304 µm/s), as shown in **Fig. 21F**.

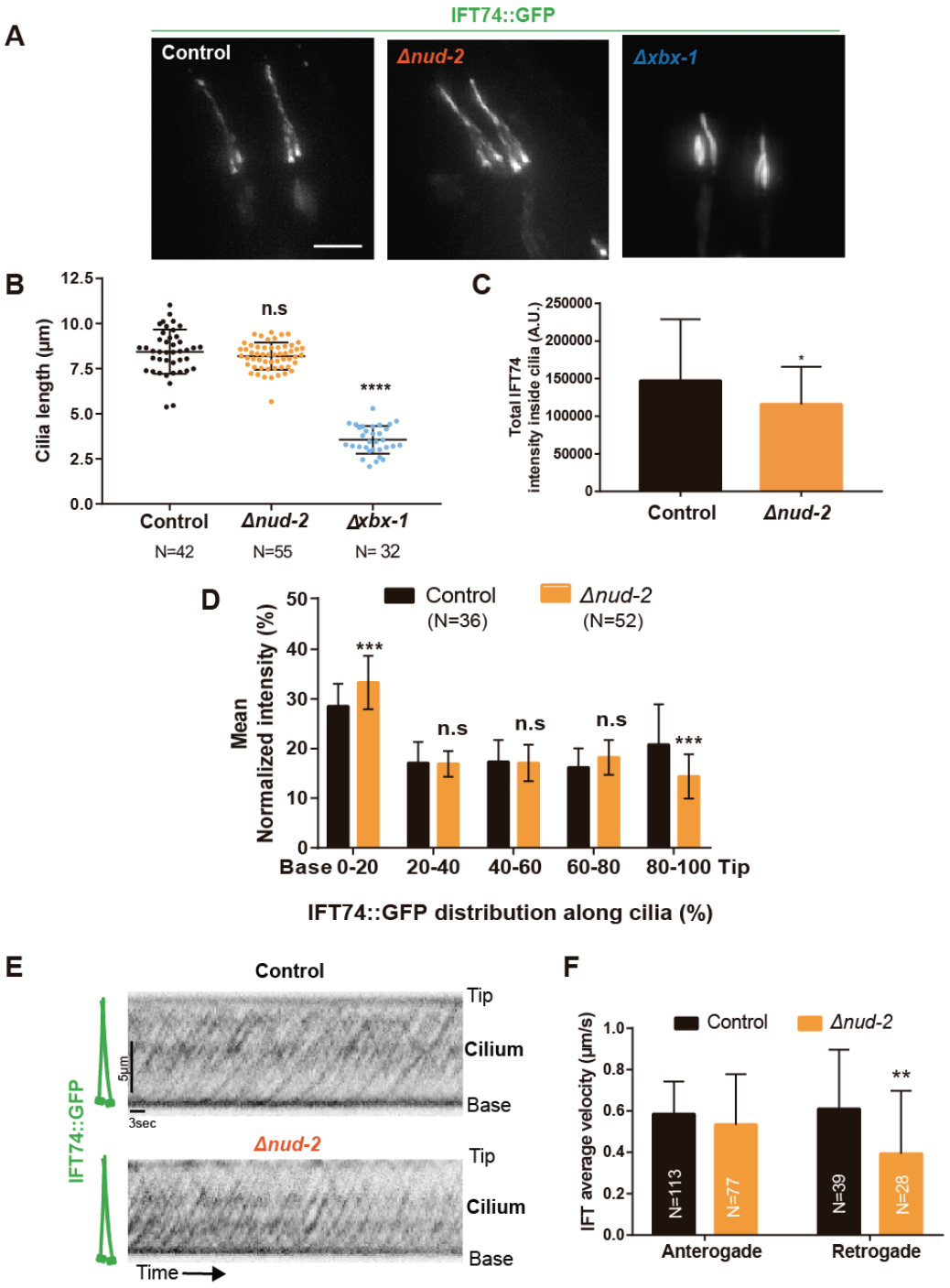

Fig. 21 – Quantifications of cilia length, IFT74 intensity and IFT74 average velocity, using IFT74::GFP as a marker. (A) Representative images of cilia in control, *Δnud-2* and *Δxbx-1* worms, visualized with IFT74::GFP. Scale bar = 5 µm. **(B)** Quantifications of cilia length. Statistical test: one way ANOVA (multiple comparisons to control. **(C)** Quantifications of IFT74::GFP total intensity in cilia. Statistical test – t-test with Welch's correction. **(D)** Quantifications of IFT74::GFP distribution along cilia. Statistical test – Multiple t-tests. **(E)** Example kymographs for control and *Δnud-2*. Scale bar: time = 3 sec and length = 5 µm. **(F)** Analysis of IFT74 particle kinetics. Statistical test – Multiple t-tests. *p<0.05, **p<0.01, ***p<0.001 and ****p<0.0001.

2.5. Sensory neurons dendrites have regular length in *Δnud-2* worms

As IFT74:GFP is also expressed in the sensory neurons dendrites, we could also measure the distance between the end of cilia until the start of the soma. We observed that loss of NUD-2 did not lead to significant differences in the dendrite's length of the phasmid PHA/B sensory neurons, when compared with controls **(Fig. 22)**. Also, the localization of the neurons soma and position of cilia seems to be normal, although is not easy to analyze and compare because of the different positions of the worms on the slide pad.

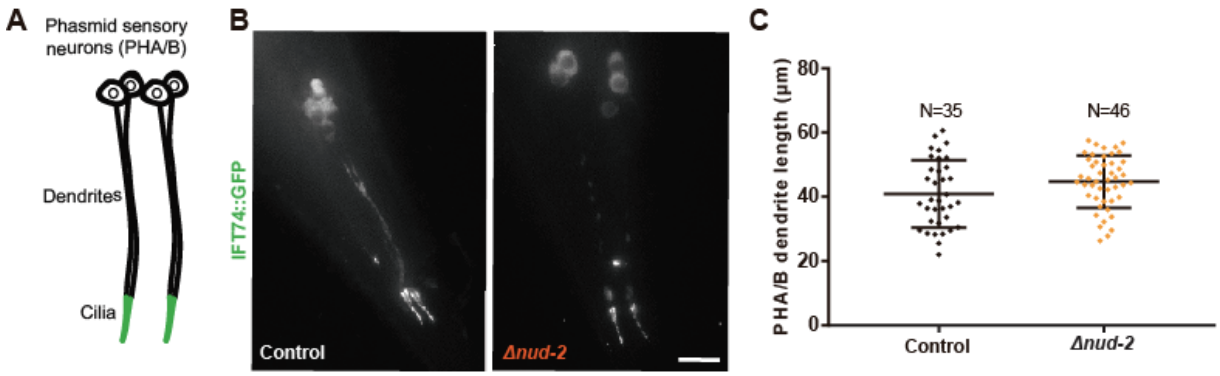

Fig. 22 – Measurement of dendrites length in phasmid sensory neurons. (A) Schematics of phasmid sensory neurons displaying soma, dendrite and cilia. **(B)** Representative images of phasmid sensory neurons in control and *Δnud-2* and *Δxbx-1* worms. Scale bar = 10 µm. **(C)** Quantifications of PHA/B dendrite length. Statistical test: t-test with Welch's correction

2.6. Cilia ultrastructure visualized by transmission electron microscopy (TEM)

In *C. elegans*, cilia can be divided in four major regions: distal segment, a middle segment (major region, that has nine doublet of microtubules), transition zone (base) and periciliary membrane compartment, as shown in **Fig. 23A** [59].

In collaboration with i3S HEMS - Histology and Electron Microscopy facility, we observed cilia ultrastructure by TEM in control and *Δnud-2* worms. As preliminary analyzes, we started by trying to find the middle segment of cilia, to study microtubule organization in *Δnud-2* mutant.

As shown in **Fig. 23B**, our preliminary results show that loss of NUD-2 does not seem to affect the normal organization of microtubules in the cilia axonemes, because we can observe nine pairs of microtubules doublets.

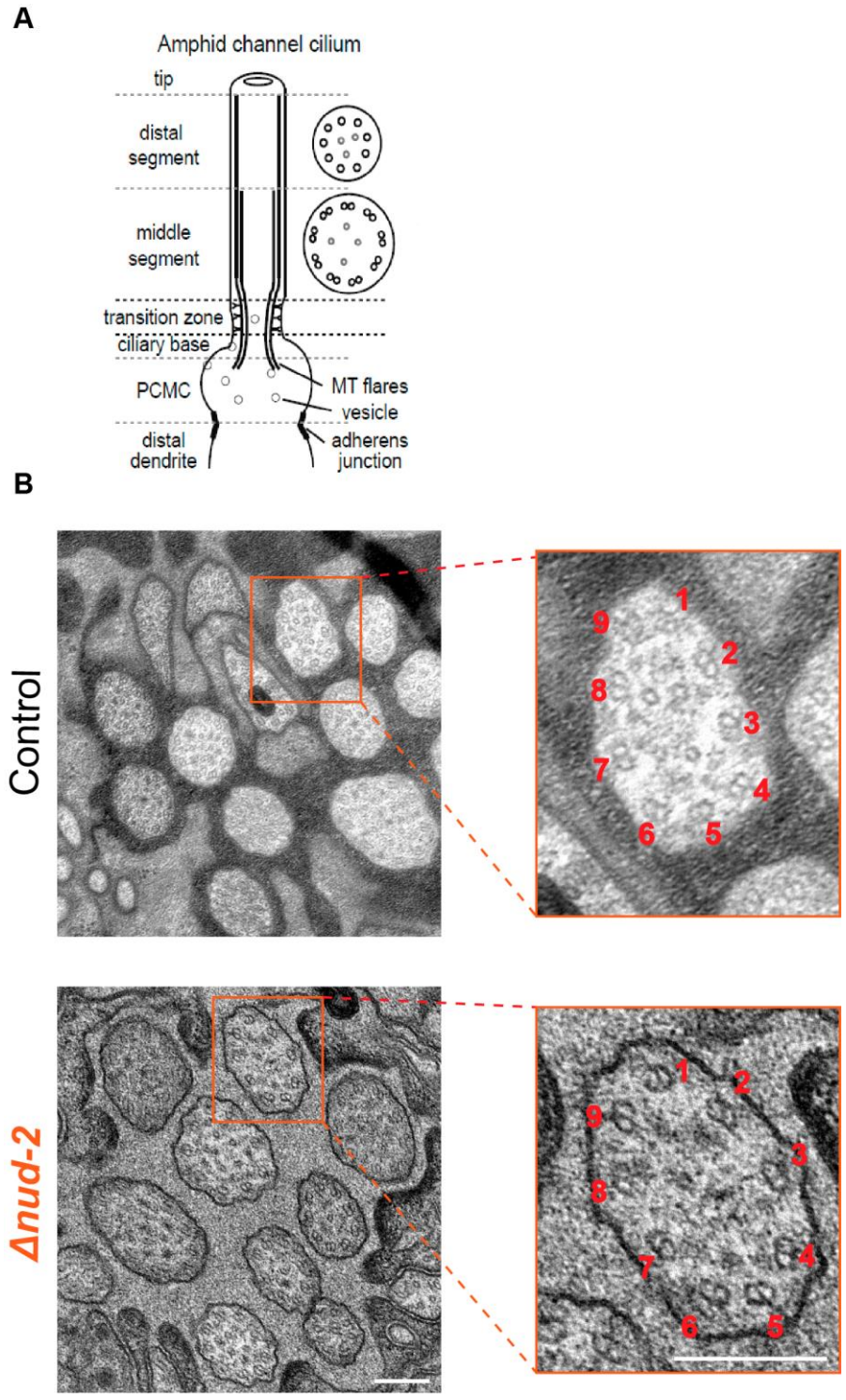

Fig. 23 – *C. elegans* ciliary ultrastructure. (A) Schematic showing the different segments of an amphid channel cilium. Adapted from [60]. **(B)** Transversal section of amphid head cilia in control (N2) and *Δnud-2* worms, showing the middle segment or beginning of transition zone of cilia, region characterized by 9 doublets of microtubules at the periphery. Scale bars = 200 nm.

2.7. CHE-3 and XBX-1 colocalize inside cilia and can be used as cilia markers

We wanted to look directly at the recruitment of Dynein-2 HC in the cilia of Δ*nud-2*. Unfortunately, the GFP::*che-3* knockin is in the same chromosome of *nud-2,* making it really hard to combine this marker with the Δ*nud-2* strain. As an alternative we decided to analyze Dynein-2 LIC (XBX-1) recruitment to cilia in the absence of NUD-2 **(Fig. 24A)**. However, we first wanted to confirm if XBX-1 could represent Dynein-2 HC (CHE-3) inside cilia. For that we first analyzed whether XBX-1::RFP and GFP::CHE-3 colocalize inside cilia using a strain that expressed fluorescent markers for both Dynein-2 subunits **(Fig. 24B)**.

Using Image J we made line scan profiles of the distribution of XBX-1 and CHE-3 **(Fig. 24C)**. Because we observed similar distribution pattern in cilia a very high degree of colocalization we concluded that XBX-1 can be used as a marker for Dynein-2 motor **(Fig. 24C)**. Also, XBX-1::RFP marker strain can be crossed into the Δ*nud-2* background strain, as these modifications are on different chromosomes (V and I, respectively).

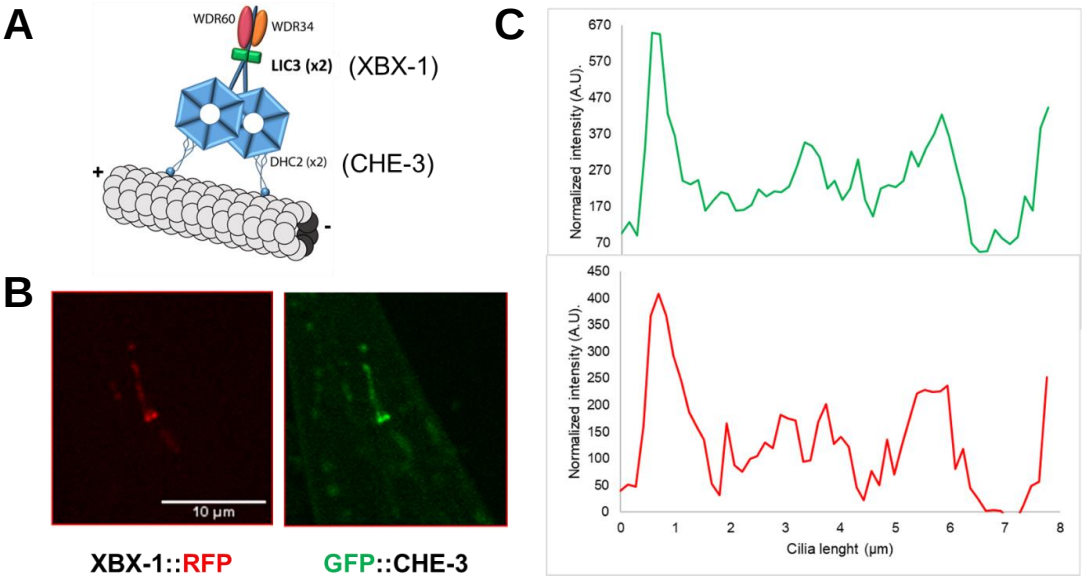

Fig. 24 – Dynein-2 HC (CHE-3) and LIC (XBX-1) colocalize inside cilia. (A) Schematic representation of Dynein-2. **(B)** Representative microscopy image of XBX-1::RFP and GFP::CHE-3. Scale bar = 10 µm. **(C)** Intensity plots for XBX-1::RFP and GFP::CHE-3.

2.8. Loss of NUD-2 does not affect Dynein-2 recruitment to cilia

Since transport inside cilia seems affected by loss of Δ*nud-2*, we wanted to verify if this defect could be caused by problems in Dynein-2 recruitment to cilia. After crossing our mutant Δ*nud-2* with a XBX-1::RFP knock-in strain (marking Dynein-2 LIC), we found that total XBX-1::RFP signal inside cilia was not significantly changed, in Δ*nud-2* cilia, meaning that the problems found in IFT are not due to ineffective recruitment of Dynein-2 to cilia **(Fig. 25)**.

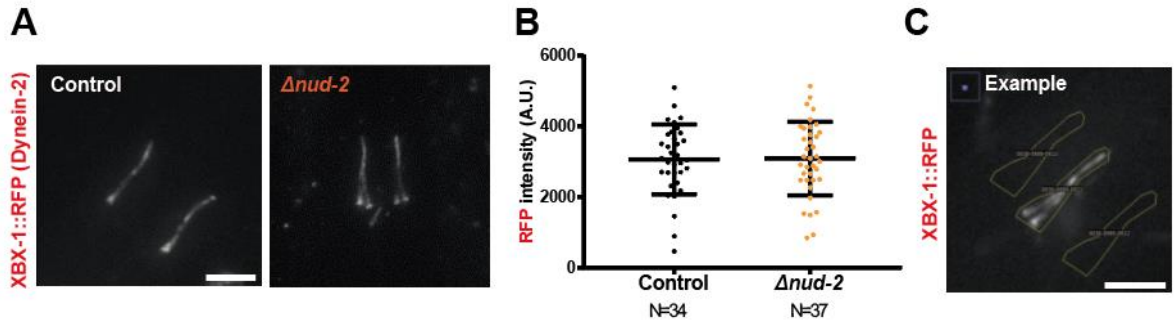

Fig. 25 – XBX-1::RFP intensity in phasmid cilia. (A) Representative cilia of controls and *Δnud-2*, marked with RFP. Scale bar = 5 µm. **(B)** Quantification of RFP total intensity. Statistical test: t-test with Welch's correction. **(C)** Example of how RFP total intensity was quantified.

In another project from our group, another subunit of Dynein-2, WDR60 (Dynein-2 IC), was labeled with GFP. WDR60::3xFlag::GFP was created by CRISPR-Cas9. Crossing this strain with the *Δnud-2* strain, we could study the WDR60 signal distribution along cilia in our mutant. Preliminary results, displayed on **Fig. 26**, show an increase in WDR60::3xFlag::GFP signal at the base of cilia, similar to the phenotype showed earlier, displayed by IFT74::GFP

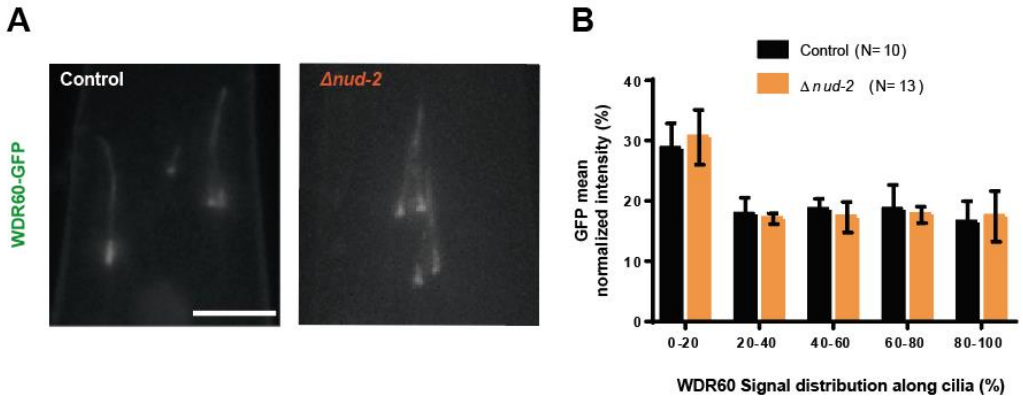

Fig. 26 – WDR60::3xFlag::GFP intensity in phasmid cilia. (A) Representative cilia of controls and *Δnud-2*, marked with GFP. Scale bar = 5 µm. **(A)** Quantification of WDR60 signal distribution along cilia. Statistical test: Multiple t tests.

2.9. The effects of NUD-2 loss in behaviors dependent on cilia-mediated signaling

As explained earlier, *C. elegans* sensory neurons are responsible for simple behaviors like finding food, avoiding obnoxious environmental conditions, worm's development and mating. Most of these behaviors are related with worm's ability to sense chemical signals from the environment in a process designated chemosensation. *C. elegans* uses chemosensation to identify its food source, driven by attractive volatile cues.

To study chemotaxis in the *Δnud-2* mutant we establish a collaboration with Dr. Neide Vieira (ICVS-Braga) and studied the chemotaxis behavior to two different volatile attractants: Isoamyl alcohol and Diacetyl that are perceived by the AWC and AWA head sensory neurons, respectively [61].

In **Fig. 27** it is shown some preliminary results for the chemotaxis assay, for two sets of experiments. If the chemotaxis index is near to 1.0, this represents a strong attraction to the chemical; a chemotaxis index close to zero indicates that the odorant is neutral to worms; and a negative chemotaxis index suggests that animals are being repelled by the odorant.

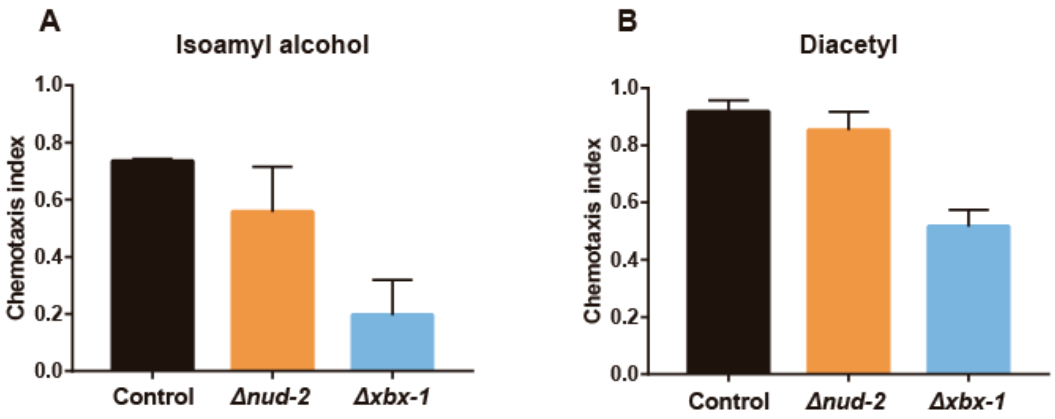

Fig. 27 – Behavioral chemotaxis characterization of *Δnud-2* mutant. (A) Isoamyl alcohol and **(B)** Diacetyl. Chemotaxis index was calculated as adults at the attractant minus the number of worms at the control, divided by the total number of worms in the plate. This assay was performed by Dr. Neide Vieira (ICVS-Braga). Only two experiments are shown so no statistics were done.

In *Δnud-2* mutant worms, it was possible to observe a slight decrease on the chemotaxis index of the odorant isoamyl alcohol, which was not observed with diacetyl. Loss of *xbx-1* caused a big defect on chemotaxis, in the perception of both odorants **(Fig. 27)**. Nevertheless, more repetitions should be conducted, as we saw that these behavioral assays can be variable.

To further study if NUD-2 was affecting cilia-mediated processes in *C. elegans*, we analyzed male worms for their mating efficiency. Male mating behaviors, in particular mate finding and vulva location are mediated through ciliated neurons located in specialized rays in the male tail **(Fig. 28)** [62].

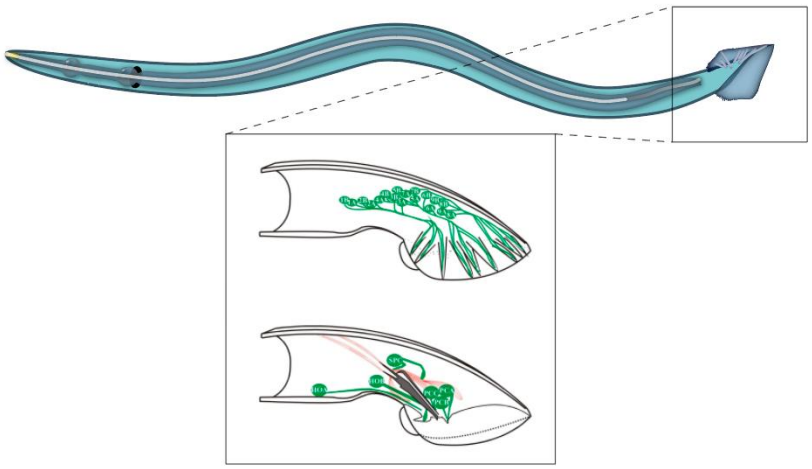

Fig. 28 – Male mating behavior relies on sensory ciliated neurons at the ray tail. Several male-specific ciliated neurons connect to muscle and other regions to activate specific male mating behaviors such as response to hermaphrodite, turning behavior and vulva location. Adapted from [62].

We took advantage of the already existing strain OE3002 (*him-8 (e1489)* IV; *xbx-1 (ok279)* V), that spontaneously generates a high percentage of males (up to 30%) to generate *him-8 (e1489)* males that could be crossed with *Δnud-2* hermaphrodites, and therefore, generate a Δ*nud-2/ him-8 (e1489)* strain that produces high number of males.

As normal controls for mating we used *him-8 (e1489)*. As males from the OE3002 (*him-8 (e1489)* IV; *xbx-1 (ok279)* V) strain are characterized by reduced mating efficiency [58] and by males tending to leave the plate, we used this strain as a control for defects in matting.

In this assay, we evaluated three parameters: whether males escape from the mating plate; males ability to mate (by verifying the presence of males in the progeny) and mating efficiency (by measuring the ratio of hermaphrodites and males in the progeny) **(Fig. 29)**.

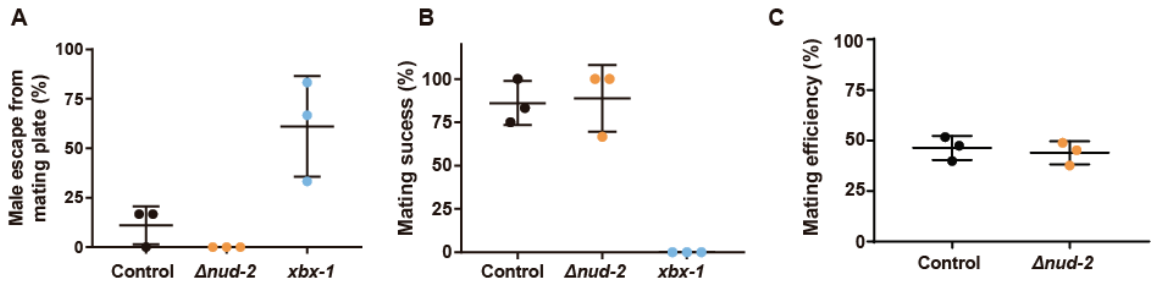

Fig. 29 – Mating assay to test *Δnud-2* males mating ability. (A) Quantification of male escape during the mating period on the mating plate. **(B)** Mating success – score of 0% (no mating) or 100% (mating) for each hermaphrodite singled out. **(C)** Mating efficiency - percentage of male progeny divided by total progeny (only for plates that presented males in the progeny). Statistical test: one-way ANOVA nonparametric – Multiple comparisons to control (low N).

First, we found that Δ*nud-2* male worms stayed in the mating plate during the 24 hours of the mating assay, a different behavior of Δ*xbx-1* males that escaped easily from the mating plate **(Fig. 29A)**. Also, Δ*nud-2* male worms were able to perform mating as efficiently as control worms, since we could observe males in the progeny, at a ~ 45% ratio **(Fig. 29B and 29C)**. In contrast, Δ*xbx*-1 did not mate at all, as no male progeny was found in the single out plates, perhaps because they tended to escape from the mating plates **(Fig. 29B)**.

DISCUSSION AND FUTURE PERSPECTIVES

In severe cases of microcephaly, such as those associated with mutations in the *NDE1* gene, neuronal progenitors become trapped at multiple stages of the cell cycle, losing their ability to generate new cells that would populate the neocortex. Co-depletion of both *NDE1* and its paralog *NDEL1* result in a striking G1 cell cycle arrest of RGPs due to defects in primary cilium resorption. Remarkably, inhibition of cilia assembly circumvents this G1 arrest, demonstrating the existence of a cilium-dependent mechanism of cell cycle control in RGPs.

This project aimed to dissect the molecular mechanisms involved in this cilium-dependent arrest of RGPs at the G1-to-S transition as well as study the involvement of well-known NDE1 interactors – LIS1 and Dynein-1 in this arrest.

Our *in utero* electroporation results suggest that the Dynein-1 regulator LIS1 is required for all NDE1 functions in the RGPs cell cycle, including in the cilium-dependent G1-to-S transition. Knowing that in this case RGPs are getting arrested early in the cell cycle, we think that they are not able to proceed in the cell, and, therefore, the mitotic index should decrease. It will be interesting to also perform immunostaining with pH3, as a way to access mitotic index. We should also stain for cilia markers, such as Arl13B, as we expect a similar phenotype to the double KD of NDE1 and NDEL1, with the presence of longer cilia. These experiments provide a new insight into the relationship between NDE1-LIS1 in the RGPs cell cycle.

We observed an even higher CyclinD1 index, when compared with the double knockdown, which suggests that the NDE1-LIS1 mutant may be even more prejudicial to the system, than not having NDE1 at all. Perhaps the presence of a form of NDE1 that can be recruited to the desired places, but cannot perform its normal function because it is unable to bind LIS1 is highly detrimental.

As a previous study showed, depletion of LIS1 causes accumulation of RGPs in the SVZ and problems in several pathways of neuronal migration [35]. However, it was not studied if this accumulation of RGPs was caused by defects in the G1-to-S transition. Actually, it will be interesting to perform *in utero* electroporation with LIS1 shRNAs and quantify the CyclinD1 index, as well as stain with cilia markers, as LIS1 KD might affect cilia length. In fact, Li *et al.*, (2015) work in *C. elegans,* showed that

GFP::LIS-1 was observed inside cilia and conditional knockouts of LIS1 resulted in dye filling defects and decreased cilia length, suggesting a role for LIS1 in regulation of cilia dynamics, by regulation of Dynein-2 [63]. Our *in utero* electroporation data also suggests that LIS1 might affect cilia dynamics, working cooperatively with NDE1. However, so far, we have no proves that these phenotypes are due to problems in IFT, as we cannot neglect the contribution of LIS1 to Dynein-1 function. We think that ciliary proteins need to be transport to the base of cilia by Dynein-1 and problems in this motor normal function may also result in abnormal cilia dynamics.

Relatively to the other mutant, overexpression with NDE1-Dynein-1 MUT could rescue the G1 accumulation observed in the double knockdown of NDE1 and NDEL1, to values similar to the control and full length NDE1 overexpression, which suggest that NDE1 does not work with Dynein-1, in the regulation of the G1-to-S transition. Still, cells are not migrating back to the VS. We believe that RGPs are probably getting arrested in G2, as NDE1 is needed to associate and recruit Dynein-1 to the nuclear envelop to perform nuclear transport (INM), as described by Hu *et al.*, (2013) [10]. In order to confirm the hypothesis that cells are getting arrested in late G2, we could stain for Geminin, a marker for S/G2 marker. To better characterize these mutants, we could also perform live imaging as a way to access INM in radial glial progenitors.

We decided to perform rescue experiments in this work, as a way to understand if overexpression of NDE1 unable to bind LIS1 or Dynein-1 was enough to overcome the double knockdown phenotype. Another option for this work would be to only perform overexpression of the mutant constructs, as they may behave as dominant negatives.

Interestingly, rescue with mutant NDE1-LIS1 or NDE1-Dynein-1 resulted in appearance of fewer RGPs at the VS, probably indicating that RGPs were prematurely differentiating in neurons, or dying. As a consequence, this made it more difficult to study if the normal cell cycle of RGPs was being affected by electroporation with our mutants.

In the second part of this thesis, our *C. elegans* work aimed to study if the NDE1 ortholog (NUD-2) regulates Dynein-2 function or recruitment, and therefore, cilium assembly and IFT. In order to study the role of NUD-2 in cilia formation and cilia-mediated signaling, we used an already existing *nud-2* knockout strain.

So far, our results indicate that Dynein-2 function and recruitment is not very affected by loss of NUD-2. Loss of NUD-2 does not seem to affect cilia ability to be

formed, morphology and structure. In this mutant, cilia length of phasmid sensory cilia is comparable to controls and Dynein-2 LIC recruitment to cilia is also not different.

Loss of NUD-2 caused some defects on IFT74 distribution along cilia, resulting in an increase in IFT74 signal at the base of the cilia and a decrease near the tip. Overall, IFT74 total intensity was decreased inside cilia. Furthermore, after studying the kinetics of the IFT74 particle, we observed a reduction in retrograde IFT74 average velocity. This result may indicate that loss of NUD-2 causes some dysregulation of anterograde and retrograde transport. More examples should be imaged, as a way to obtain a higher N. Another parameter, such as IFT frequency, should also be analyzed in this context.

In the *Δnud-2* cilia, IFT74 distribution shows an unexpected trend with increase in intensity at the base of cilia, opposed from what we were expecting, that if NUD-2 was playing a role in retrograde transport, we would expect to see an accumulation of IFT particles at the tip of cilia in our mutant. In *C. elegans*, it seems that problems in retrograde transport caused by knockout of essential parts of the retrograde machinery results in a range of phenotypes. Loss of XBX-1 (Dynein-2 LIC), subunit essential for the stabilization of Dynein-2, causes an enormous unbalance in anterograde and retrograde transport and results in an accumulation of IFT particles in base of cilia, giving a phenotype of stumpy and bulged cilia [58]. Similarly, mutations in IFT-139, a component of the retrograde IFT-A subcomplex in *C. elegans*, had abnormal short and stumpy cilia [64].

Loss of NUD-2 seems to affect IFT74 presence in cilia, distribution and velocity inside cilia, suggesting a potential role for NUD-2 in cilia dynamics, but these results cannot show a direct relation between NUD-2 and Dynein-2. In this case, we cannot exclude that these phenotypes can be due to improper function of Dynein-1, in the retrograde transport of ciliary proteins to cilia base. In accordance with this theory, Wenjing *et al.*, (2017) found that mutations in Dynein-1 blocked centriole translocation along the phasmid neurons dendrites that inhibited ciliogenesis. Conditional mutations in *dhc-1* and *dlc-1* (Dynein-1 HC and LC8, respectively) cause a decrease in cilia length and lead to a dye filling defect phenotype [65]. Interestingly, Kim *et al.*, (2011) uncovered that LC8 overexpression (light chain shared by both Dynein-1 and Dynein-2) can overcome the stumpy cilia phenotype induced by NDE1 overexpression, suggesting that NDE1 negatively regulates ciliary length through mechanisms involving LC8 [49]. We could test this hypothesis using *in utero* electroporation

technique to overexpress a mutant construct of NDE1 that cannot bind LC8. We already have this construct at the lab, but still needs to be validated by biochemical assays. With this construct, we could study the cilia and RGPs cell cycle effects of having a form of NDE1 that cannot bind LC8.

Because we saw differences in IFT, we analyzed cilia-related processes like mating behavior and chemotaxis. Loss of NUD-2 did not cause any major defect on worm's normal behavior, as worms could still perform mating and search for attractive odorants. In *C. elegans*, neuronal transmission start with the sensory neurons that synapse with interneurons, which in turn synapse with motor neurons, responsible for worms behaviors. In this study, we did not test other cilia-mediated processes, so we still want to test if loss of NUD-2 can be affecting other neuronal pathways downstream of sensory cilia, such as synapses and projections to the interneurons and motor GABAergic neurons.

Our *C. elegans* experiments suggests that NUD-2 is mostly dispensable for Dynein-2 function and recruitment to cilia, and, moreover, they indicate that cilia-mediated signaling responsible for normal worm behavior is mostly normal, in these mutant worms. With this study, we could not establish NUD-2 as a regulator of Dynein-2, but we have some evidences that NUD-2 might regulate cilia dynamics, but the mechanisms are poorly understood. In the future, it will be necessary to test if NDE1 can associate with Dynein-2, using *in vitro* biochemical assays. Detection of an interaction would support a role for NDE1 in Dynein-2 function.

Last, our data in neural progenitors provides new insights into how NDE1 and its binding partners contribute to the functions of cytoplasmic Dyneins during brain development. Our work in *C. elegans*, consolidate *C. elegans* as a powerful model to study cilia dynamics and neuronal networks. We hope that continuing this work will help unveiling the mechanisms involved in the NDE1-associated microcephaly.

REFERENCES

1. Barry, D. S., Pakan, J. M., and McDermott, K. W., *Radial glial cells: key organisers in CNS development.* Int J Biochem Cell Biol, 2014. **46**: p. 76-9.
2. Stiles, J. and Jernigan, T. L., *The basics of brain development.* Neuropsychology review, 2010. **20**(4): p. 327-48.
3. Dantas, T. J., Carabalona, A., Hu, D. J., et al., *Emerging roles for motor proteins in progenitor cell behavior and neuronal migration during brain development.* Cytoskeleton (Hoboken), 2016. **73**(10): p. 566-576.
4. Laguesse, S., Peyre, E., and Nguyen, L., *Progenitor genealogy in the developing cerebral cortex.* Cell Tissue Res, 2015. **359**(1): p. 17-32.
5. Hall, A. K. and Miller, R. H., *Stem Cells in the Nervous System*, in *Basic Neurochemistry*, Brady, S. T., Siegel, G. J., Albers, R. W., et al., Editors. 2012, Academic Press: New York. p. 558-568.
6. Bear, M. F., Connors, B. W., and Paradiso, M. A., *Neuroscience : exploring the brain*. 3rd ed. 2007: Philadelphia.
7. *Motor Proteins*, in *Cell Biology*, Pollard, T. D., Earnshaw, W. C., Lippincott-Schwartz, J., et al., Editors. 2017, Elsevier. p. 623-638.
8. Tortosa, E., Kapitein, L. C., and Hoogenraad, C. C., *Microtubule Organization and Microtubule-Associated Proteins (MAPs)*, in *Dendrites*, Emoto, K., Wong, R., Huang, E., et al., Editors. 2016, Springer Japan: Tokyo. p. 31-75.
9. Del Bene, F., *Interkinetic nuclear migration: cell cycle on the move.* EMBO J, 2011. **30**(9): p. 1676-7.
10. Hu, D. J., Baffet, A. D., Nayak, T., et al., *Dynein recruitment to nuclear pores activates apical nuclear migration and mitotic entry in brain progenitor cells.* Cell, 2013. **154**(6): p. 1300-13.
11. Spear, P. C. and Erickson, C. A., *Interkinetic nuclear migration: a mysterious process in search of a function.* Dev Growth Differ, 2012. **54**(3): p. 306-16.
12. Sauer, F. C., *Mitosis in the neural tube.* Journal of Comparative Neurology, 1935. **62**(2): p. 377-405.
13. Tsai, J. W., Lian, W. N., Kemal, S., et al., *Kinesin 3 and cytoplasmic dynein mediate interkinetic nuclear migration in neural stem cells.* Nat Neurosci, 2010. **13**(12): p. 1463-71.
14. Baffet, A. D., Hu, D. J., and Vallee, R. B., *Cdk1 Activates Pre-mitotic Nuclear Envelope Dynein Recruitment and Apical Nuclear Migration in Neural Stem Cells.* Dev Cell, 2015. **33**(6): p. 703-16.
15. Doobin, D. J., Kemal, S., Dantas, T. J., et al., *Severe NDE1-mediated microcephaly results from neural progenitor cell cycle arrests at multiple specific stages.* Nat Commun, 2016. **7**: p. 12551.
16. Gibbons, I. R. and Rowe, A. J., *Dynein: A Protein with Adenosine Triphosphatase Activity from Cilia.* Science, 1965. **149**(3682): p. 424-6.
17. Gibbons, I. R., *Studies on the Protein Components of Cilia from Tetrahymena Pyriformis.* Proc Natl Acad Sci U S A, 1963. **50**(5): p. 1002-10.

18. Paschal, B. M. and Vallee, R. B., *Retrograde transport by the microtubule-associated protein MAP 1C.* Nature, 1987. **330**(6144): p. 181-3.
19. Roberts, A. J., Kon, T., Knight, P. J., et al., *Functions and mechanics of dynein motor proteins.* Nat Rev Mol Cell Biol, 2013. **14**(11): p. 713-26.
20. Wickstead, B., *The evolutionary biology of dyneins*, in *Dyneins*, King, S. M., Editor. 2018, Academic Press. p. 100-138.
21. Reck-Peterson, S. L., Redwine, W. B., Vale, R. D., et al., *The cytoplasmic dynein transport machinery and its many cargoes.* Nat Rev Mol Cell Biol, 2018. **19**(6): p. 382-398.
22. Cianfrocco, M. A., DeSantis, M. E., Leschziner, A. E., et al., *Mechanism and regulation of cytoplasmic dynein.* Annual review of cell and developmental biology, 2015. **31**: p. 83-108.
23. Bradshaw, N. J. and Hayashi, M. A., *NDE1 and NDEL1 from genes to (mal)functions: parallel but distinct roles impacting on neurodevelopmental disorders and psychiatric illness.* Cell Mol Life Sci, 2017. **74**(7): p. 1191-1210.
24. Bradshaw, N. J., Hennah, W., and Soares, D. C., *NDE1 and NDEL1: twin neurodevelopmental proteins with similar 'nature' but different 'nurture'.* Biomol Concepts, 2013. **4**(5): p. 447-64.
25. Wynne, C. L. and Vallee, R. B., *Cdk1 phosphorylation of the dynein adapter Nde1 controls cargo binding from G2 to anaphase.* J Cell Biol, 2018. **217**(9): p. 3019-3029.
26. Feng, Y. and Walsh, C. A., *Mitotic spindle regulation by Nde1 controls cerebral cortical size.* Neuron, 2004. **44**(2): p. 279-93.
27. Sasaki, S., Mori, D., Toyo-oka, K., et al., *Complete loss of Ndel1 results in neuronal migration defects and early embryonic lethality.* Mol Cell Biol, 2005. **25**(17): p. 7812-27.
28. Wynshaw-Boris, A., *Lissencephaly and LIS1: insights into the molecular mechanisms of neuronal migration and development.* Clin Genet, 2007. **72**(4): p. 296-304.
29. Dujardin, D. L. and Vallee, R. B., *Dynein at the cortex.* Current Opinion in Cell Biology, 2002. **14**(1): p. 44-49.
30. McKenney, R. J., Vershinin, M., Kunwar, A., et al., *LIS1 and NudE induce a persistent dynein force-producing state.* Cell, 2010. **141**(2): p. 304-14.
31. Htet, Z. M., Gillies, J. P., Baker, R. W., et al., *Lis1 promotes the formation of maximally activated cytoplasmic dynein-1 complexes.* bioRxiv, 2019: p. 683052.
32. Elshenawy, M. M., Kusakci, E., Volz, S., et al., *Lis1 activates dynein motility by pairing it with dynactin.* bioRxiv, 2019: p. 685826.
33. Qiu, R., Zhang, J., and Xiang, X., *Insights into LIS1 function in cargo-adapter-mediated dynein activation in vivo.* bioRxiv, 2019: p. 683995.
34. Cahana, A., Escamez, T., Nowakowski, R. S., et al., *Targeted mutagenesis of Lis1 disrupts cortical development and LIS1 homodimerization.* Proc Natl Acad Sci U S A, 2001. **98**(11): p. 6429-34.
35. Tsai, J. W., Chen, Y., Kriegstein, A. R., et al., *LIS1 RNA interference blocks neural stem cell division, morphogenesis, and motility at multiple stages.* J Cell Biol, 2005. **170**(6): p. 935-45.
36. Plotnikova, O. V., Pugacheva, E. N., and Golemis, E. A., *Primary cilia and the cell cycle.* Methods Cell Biol, 2009. **94**: p. 137-60.

37. Hou, Y. and Witman, G. B., *Dynein and intraflagellar transport.* Exp Cell Res, 2015. **334**(1): p. 26-34.

38. Rajagopalan, V., D'Amico, J. P., and Wilkes, D. E., *Cytoplasmic dynein-2: from molecules to human diseases.* Frontiers in Biology, 2012. **8**(1): p. 119-126.

39. Witman, G. B. and Hou, Y., *Dynein and intraflagellar transport*, in *Dyneins*, King, S. M., Editor. 2018, Academic Press. p. 386-432.

40. Toropova, K., Mladenov, M., and Roberts, A. J., *Intraflagellar transport dynein is autoinhibited by trapping of its mechanical and track-binding elements.* Nature Structural & Molecular Biology, 2017. **24**(5): p. 461-468.

41. Lechtreck, K. F., *IFT-Cargo Interactions and Protein Transport in Cilia.* Trends in biochemical sciences, 2015. **40**(12): p. 765-778.

42. Waters, A. M. and Beales, P. L., *Ciliopathies: an expanding disease spectrum.* Pediatric nephrology (Berlin, Germany), 2011. **26**(7): p. 1039-56.

43. Taylor, S. P., Dantas, T. J., Duran, I., et al., *Mutations in DYNC2LI1 disrupt cilia function and cause short rib polydactyly syndrome.* Nat Commun, 2015. **6**: p. 7092.

44. Barkovich, A. J., Guerrini, R., Kuzniecky, R. I., et al., *A developmental and genetic classification for malformations of cortical development: update 2012.* Brain, 2012. **135**(Pt 5): p. 1348-69.

45. Faheem, M., Naseer, M. I., Rasool, M., et al., *Molecular genetics of human primary microcephaly: an overview.* BMC Med Genomics, 2015. **8 Suppl 1**(1): p. S4.

46. Abdel-Hamid, M. S., El-Dessouky, S. H., Ateya, M. I., et al., *Phenotypic spectrum of NDE1-related disorders: from microlissencephaly to microhydranencephaly.* Am J Med Genet A, 2019. **179**(3): p. 494-497.

47. Alkuraya, F. S., Cai, X., Emery, C., et al., *Human mutations in NDE1 cause extreme microcephaly with lissencephaly [corrected]*. Am J Hum Genet, 2011. **88**(5): p. 536-47.

48. Li, A., Saito, M., Chuang, J. Z., et al., *Ciliary transition zone activation of phosphorylated Tctex-1 controls ciliary resorption, S-phase entry and fate of neural progenitors.* Nat Cell Biol, 2011. **13**(4): p. 402-11.

49. Kim, S., Zaghloul, N. A., Bubenshchikova, E., et al., *Nde1-mediated inhibition of ciliogenesis affects cell cycle re-entry.* Nat Cell Biol, 2011. **13**(4): p. 351-60.

50. Baffet, A. D., Carabalona, A., Dantas, T. J., et al., *Chapter 17 - Cellular and subcellular imaging of motor protein-based behavior in embryonic rat brain*, in *Methods in cell biology*, Pfister, K. K., Editor. 2016, Academic Press. p. 349-363.

51. Altun, Z. F. and Hall, D. H. *INTRODUCTION TO C. elegans ANATOMY* 2009 [cited 2018; Available from: http://www.wormatlas.org/hermaphrodite/introduction/Introframeset.html.

52. Inglis, P. N., Ou, G., Leroux, M. R., et al. *The sensory cilia of Caenorhabditis elegans*. 2006 [cited 2018; Available from: http://www.wormbook.org/chapters/www_ciliumbiogenesis.2/ciliumbiogenesis.html.

53. Neumann, S., Chassefeyre, R., Campbell, G. E., et al., *KymoAnalyzer: a software tool for the quantitative analysis of intracellular transport in neurons.* Traffic, 2017. **18**(1): p. 71-88.

54. Wang, S., Ketcham, S. A., Schon, A., et al., *Nudel/NudE and Lis1 promote dynein and dynactin interaction in the context of spindle morphogenesis.* Mol Biol Cell, 2013. **24**(22): p. 3522-33.

55. Derewenda, U., Tarricone, C., Choi, W. C., et al., *The structure of the coiled-coil domain of Ndel1 and the basis of its interaction with Lis1, the causal protein of Miller-Dieker lissencephaly.* Structure, 2007. **15**(11): p. 1467-81.

56. Simoes, P. A., Celestino, R., Carvalho, A. X., et al., *NudE regulates dynein at kinetochores but is dispensable for other dynein functions in the C. elegans early embryo.* J Cell Sci, 2018. **131**(1): p. jcs212159.

57. Tong, Y. G. and Burglin, T. R., *Conditions for dye-filling of sensory neurons in Caenorhabditis elegans.* J Neurosci Methods, 2010. **188**(1): p. 58-61.

58. Schafer, J. C., Haycraft, C. J., Thomas, J. H., et al., *XBX-1 encodes a dynein light intermediate chain required for retrograde intraflagellar transport and cilia assembly in Caenorhabditis elegans.* Mol Biol Cell, 2003. **14**(5): p. 2057-70.

59. Doroquez, D. B., Berciu, C., Anderson, J. R., et al., *A high-resolution morphological and ultrastructural map of anterior sensory cilia and glia in Caenorhabditis elegans.* eLife, 2014. **3**: p. e01948.

60. Sanders, A. A. W. M., Kennedy, J., and Blacque, O. E., *Chapter 17 - Image analysis of Caenorhabditis elegans ciliary transition zone structure, ultrastructure, molecular composition, and function*, in *Methods in cell biology*, Basto, R. and Marshall, W. F., Editors. 2015, Academic Press. p. 323-347.

61. Vieira, N., Bessa, C., Rodrigues, A. J., et al., *Sorting nexin 3 mutation impairs development and neuronal function in Caenorhabditis elegans.* Cell Mol Life Sci, 2018. **75**(11): p. 2027-2044.

62. Barr, M. M. and Garcia, L. R. *Male mating behavior* 2006; Available from: http://www.wormbook.org.

63. Li, W., Yi, P., and Ou, G., *Somatic CRISPR-Cas9-induced mutations reveal roles of embryonically essential dynein chains in Caenorhabditis elegans cilia.* J Cell Biol, 2015. **208**(6): p. 683-92.

64. Niwa, S., *The nephronophthisis-related gene ift-139 is required for ciliogenesis in Caenorhabditis elegans.* Sci Rep, 2016. **6**: p. 31544.

65. Li, W. J., Yi, P. S., Zhu, Z. W., et al., *Centriole translocation and degeneration during ciliogenesis in Caenorhabditis elegans neurons.* Embo Journal, 2017. **36**(17): p. 2553-2566.

66. Cox, J., Jackson, A. P., Bond, J., et al., *What primary microcephaly can tell us about brain growth.* Trends Mol Med, 2006. **12**(8): p. 358-66.

67. Bilguvar, K., Ozturk, A. K., Louvi, A., et al., *Whole-exome sequencing identifies recessive WDR62 mutations in severe brain malformations.* Nature, 2010. **467**(7312): p. 207-10.

68. Kraemer, N., Issa, L., Hauck, S. C., et al., *What's the hype about CDK5RAP2?* Cell Mol Life Sci, 2011. **68**(10): p. 1719-36.

69. Thornton, G. K. and Woods, C. G., *Primary microcephaly: do all roads lead to Rome?* Trends Genet, 2009. **25**(11): p. 501-10.

SUPPLEMENTARY DATA

Table S1 – Microcephaly associated genes.

Gene	Processes	Effect on brain development	Reference
Microcephalin (MCPH1)	DNA damage-induced responses Chromosome condensation G2/M checkpoint arrest	Decrease in the cortex layer II-III Normal neuronal migration	[45, 66]
WDR62 (MCPH2)	Neuronal development Spindle poles of diving cells	Decrease in progenitor's proliferation, defective spindle orientation, reduced centrosome integrity and problems in mitosis.	[45, 67]
CDK5RAP2 (MCPH3)	Microtubule and centrosome dynamics Spindle checkpoint	Decrease in progenitor pool (interfere with symmetric divisions) Reduce cell survival	[45, 68]
ASPM	Mitotic spindle	Influence the orientation of the mitotic spindle and progenitor's cell division fate	[45, 69]
NDE1/NDEL1	Mitosis, nuclei positioning (dynein-mediated) and cell migration	Defects in progenitor's cell cycle (inability of progenitors to ever reach mitosis) Neurons cannot reach the cortical plate	[15, 47]
CENPJ	Centrosome and microtubules function	Mitosis arrest and formation of multipolar spindles	[45]
CEP135	Centrosome and miotic splindles	Disorganized microtubules	[45]

STIL	Mitotic entry, apoptosis regulation and centrosome function	Apoptosis, reduced proliferation and abnormal expression of several essential genes	[45]

FACULDADE DE **MEDICINA**